NAVAL POSTGRADUATE SCHOOL

MONTEREY, CALIFORNIA

THESIS

COMPARISON OF COMPLEMENTARY SEQUENCES IN HYBRID PHASE AND FREQUENCY SHIFT KEYING CW RADAR USING PERIODIC AMBIGUITY ANALYSIS

by

Francisco José Castañeda

December 2012

Thesis Advisor: Phillip E. Pace
Co-Advisor: Richard Harkins

Approved for public release; distribution is unlimited

THIS PAGE INTENTIONALLY LEFT BLANK

REPORT DOCUMENTATION PAGE			Form Approved OMB No. 0704–0188
Public reporting burden for this collection of information is estimated to average 1 hour per response, including the time for reviewing instruction, searching existing data sources, gathering and maintaining the data needed, and completing and reviewing the collection of information. Send comments regarding this burden estimate or any other aspect of this collection of information, including suggestions for reducing this burden, to Washington headquarters Services, Directorate for Information Operations and Reports, 1215 Jefferson Davis Highway, Suite 1204, Arlington, VA 22202–4302, and to the Office of Management and Budget, Paperwork Reduction Project (0704–0188) Washington DC 20503.			
1. AGENCY USE ONLY ***(Leave blank)***	**2. REPORT DATE** December 2012	**3. REPORT TYPE AND DATES COVERED** Master's Thesis	
4. TITLE AND SUBTITLE COMPARISON OF COMPLEMENTARY SEQUENCES IN HYBRID PHASE AND FREQUENCY SHIFT KEYING CW RADAR USING PERIODIC AMBIGUITY ANALYSIS		**5. FUNDING NUMBERS**	
6. AUTHOR(S) Francisco José Castañeda			
7. PERFORMING ORGANIZATION NAME(S) AND ADDRESS(ES) Naval Postgraduate School Monterey, CA 93943–5000		**8. PERFORMING ORGANIZATION REPORT NUMBER**	
9. SPONSORING /MONITORING AGENCY NAME(S) AND ADDRESS(ES) N/A		**10. SPONSORING/MONITORING AGENCY REPORT NUMBER**	
11. SUPPLEMENTARY NOTES The views expressed in this thesis are those of the author and do not reflect the official policy or position of the Department of Defense or the U.S. Government. IRB Protocol number ____N/A____.			
12a. DISTRIBUTION / AVAILABILITY STATEMENT Approved for public release; distribution is unlimited		**12b. DISTRIBUTION CODE**	

13. ABSTRACT (maximum 200 words)

Continuous waveform (CW) polyphase sequences for radar have a much lower power spectral density (PSD) than pulsed signals but can retain the same target detection capability. The use of different phase values or subcodes to modulate the carrier provides a low probability of intercept (LPI) radar waveform which cannot be seen by a non-cooperative intercept receiver (NCIR). Also, it is a low probability of detection (LPD) waveform due to the low PSD. Frequency shift keying (FSK) radar has a higher PSD but is moved about quickly in frequency over a large bandwidth in which the NCIR cannot follow. Consequently, the FSK (usually a Costas frequency set) remains a LPI signal but not a LPD. To combine the advantages of each waveform, this thesis presents a hybrid FSK/PSK emitter waveform to further the LPI, LPD characteristics. By combining both techniques (PSK/FSK), a high time-bandwidth waveform is constructed that provides better LPI/LPD characteristics than each waveform. The periodic ambiguity function (PAF) is evaluated for three different complementary sequences to modulate a Costas frequency set. The peak time and Doppler sidelobes of the PAF are compared against the P4 polyphase modulation for the Golay complementary sequence (15 dB improvement), the quaternary periodic complementary sequence (16 dB improvement), and the quaternary Golay complementary sequence (18 dB improvement).

14. SUBJECT TERMS Continuous waveform (CW), power spectral density (PSD), non-cooperative intercept receiver (NCIR), complementary sequence, Golay code, frequency hopping, autocorrelation function (ACF), periodic ambiguity function (PAF), phase shift keying (PSK), frequency shift keying (FSK), low probability of intercept (LPI), low probability of detection (LPD).	**15. NUMBER OF PAGES** 77
	16. PRICE CODE

17. SECURITY CLASSIFICATION OF REPORT	**18. SECURITY CLASSIFICATION OF THIS PAGE**	**19. SECURITY CLASSIFICATION OF ABSTRACT**	**20. LIMITATION OF ABSTRACT**
Unclassified	Unclassified	Unclassified	UU

NSN 7540–01–280–5500 Standard Form 298 (Rev. 2–89)
Prescribed by ANSI Std. 239–18

THIS PAGE INTENTIONALLY LEFT BLANK

Approved for public release; distribution is unlimited

COMPARISON OF COMPLEMENTARY SEQUENCES IN HYBRID PHASE AND FREQUENCY SHIFT KEYING CW RADAR USING PERIODIC AMBIGUITY ANALYSIS

Francisco José Castañeda
Lieutenant, Colombian Navy
B.S., Colombian Naval Academy "Almirante Padilla," 2010

Submitted in partial fulfillment of the
requirements for the degree of

MASTER OF SCIENCE IN APPLIED PHYSICS

from the

NAVAL POSTGRADUATE SCHOOL
December 2012

Author: Francisco José Castañeda

Approved by: Phillip E. Pace
Thesis Advisor

Richard Harkins
Thesis Co-Advisor

Andres Larraza
Chair, Department of Physics

THIS PAGE INTENTIONALLY LEFT BLANK

ABSTRACT

Continuous waveform (CW) polyphase sequences for radar have a much lower power spectral density (PSD) than pulsed signals but can retain the same target detection capability. The use of different phase values or subcodes to modulate the carrier provides a low probability of intercept (LPI) radar waveform which cannot be seen by a non-cooperative intercept receiver (NCIR). Also, it is a low probability of detection (LPD) waveform due to the low PSD. Frequency shift keying (FSK) radar has a higher PSD but is moved about quickly in frequency over a large bandwidth in which the NCIR cannot follow. Consequently, the FSK (usually a Costas frequency set) remains a LPI signal but not a LPD. To combine the advantages of each waveform, this thesis presents a hybrid FSK/PSK emitter waveform to further the LPI, LPD characteristics. By combining both techniques (PSK/FSK), a high time-bandwidth waveform is constructed that provides better LPI/LPD characteristics than each waveform. The periodic ambiguity function (PAF) is evaluated for three different complementary sequences to modulate a Costas frequency set. The peak time and Doppler sidelobes of the PAF are compared against the P4 polyphase modulation for the Golay complementary sequence (15 dB improvement), the quaternary periodic complementary sequence (16 dB improvement), and the quaternary Golay complementary sequence (18 dB improvement).

THIS PAGE INTENTIONALLY LEFT BLANK

TABLE OF CONTENTS

LIST OF FIGURES

THIS PAGE INTENTIONALLY LEFT BLANK

LIST OF TABLES

THIS PAGE INTENTIONALLY LEFT BLANK

LIST OF ACRONYMS AND ABBREVIATIONS

AACF	Aperiodic Autocorrelation Function
ACF	Autocorrelation Function
ARMs	Antiradiation Missiles
BPSK	Binary Phase Shift Keying
CCF	Cross Correlation Function
CW	Continuous Waveform
CS	Complementary Sequence
EA	Electronic Attack
ERP	Effective Radiated Power
EW	Electronic Warfare
FMCW	Frequency Modulation Continuous Waveform
FH	Frequency Hopping
FSK	Frequency Shift Keying
GCS	Golay Complementary Sequence
IRE	Institute of Radio Engineers
ISL	Integrated Sidelobe Level
LPD	Low Probability of Detection
LPI	Low Probability of Intercept
LPID	Low Probability of Identification
NCIR	Non-cooperative of Intercept Receiver
PACF	Periodic Autocorrelation Function
PAF	Periodic Ambiguity Function
PCS	Periodic Complementary Sequence
PDS	Peak Doppler Sidelobes
PRI	Pulse Repetition Interval
PSD	Power Spectral Density
PSL	Peak Sidelobe Level
PSK	Phase Shift Keying
QGCS	Quaternary Golay Complementary Sequence
QPCS	Quaternary Periodic Complementary Sequence

RADAR	Radio Detection and Ranging
RF	Radio Frequency
SLR	Side Lobe Ratio
SNR	Signal-to-Noise Ratio

ACKNOWLEDGMENTS

Special thanks to Professor Phillip E. Pace, whose support, advice, dedication, and knowledge were unconditional throughout this study. In addition, my sincere appreciation to Professor Richard Harkins, whose guidance since my arrival to the Naval Postgraduate School greatly enhanced my studies on board this well recognized entity.

My everlasting gratitude to the Colombian Navy and especially to COTECMAR for the opportunity to prepare my professional expertise in subjects that directly matter to the Navy and Colombia.

Most importantly, my utmost gratitude and thanks to Monica, my wife, whose unfailing love motivates me to achieve what I had proposed, supporting those long study hours and keeping me motivated to succeed at any cost.

I would also like to thank my family back in Colombia, whose encouraging voices from the distance provided me an unending support throughout this endeavor.

Last, but not least, thanks to God, my guide and shepherd along every activity and moment in my life.

THIS PAGE INTENTIONALLY LEFT BLANK

I. INTRODUCTION

A. FSK AND PSK CODING OF LPI RADAR CW SIGNALS

Most current radars are designated to transmit short duration pulses with relatively high peak power. Modern Electronic Warfare (EW) receivers must perform the tasks of detection, parameter identification, classification, and exploitation in a complex environment of high noise interference and multiple signals [1]. The high power pulsed radars can be detected easily by the use of relatively modest EW systems. The intercept of these type of radar transmissions ultimately leads to vulnerability through the use of either anti-radiation missiles or Electronic Attack (EA). By using Low Probability of Intercept (LPI) techniques, it is possible to design radar systems which cannot be detected by current EW intercept receiver designs [2]. These radar systems use Continuous Waveform (CW) signals that are polyphase modulated and/or frequency modulated. The modulations allow the CW waveform to detect the targets but not be detected by the intercept receiver.

LPI signals are typically low power CW waveforms that are modulated by a periodic function, such as a phase code sequence or a Frequency Hopping (FH) sequence. As such, the Periodic Autocorrelation Function (PACF) and Periodic Ambiguity Function (PAF) analysis can help determine the receiver response and its measurement accuracy including the effect on target resolution, the ambiguities in range, radial velocity and its response to clutter. The PAF is similar to the ambiguity function often used to represent the magnitude of the matched receiver output for a CW modulated signal. The cut of the PAF at zero Doppler is the PACF and cuts of the PAF along the zero delay yield the response of the correlation receiver at a given Doppler shift. The time sidelobes in the PACF help quantify the LPI waveform in its ability to detect targets without interfering sidelobe targets [3]. That is, if the PACF has high sidelobes, a second nearby target might be able to hide in a sidelobe and go undetected. To quantify the LPI waveform characteristics, the Peak Side Lobe (PSL) and the Integrated Sidelobe Level (ISL) can be defined to measure both the maximum sidelobe power and the total power in the

sidelobes and is a useful measure when a single point target response is of concern. The ISL is considered a more useful measure than the PSL when distributed targets are of concern [1].

Polyphase modulations or poly-Phase Shift Keying (PSK) waveforms include binary, the Frank code, the P1, P2, P3 and P4. These CW modulations are particularly attractive for LPI radar systems as they have very low periodic ambiguity sidelobes in both time-offset and Doppler-offset. In fact, the Frank code, P1, P3 and P4 codes are "perfect codes" as they have zero level sidelobes in the PACF [3]. Note however, that finite duration signals, such as pulse train cannot achieve this ideal autocorrelation function since as the first sample (or last sample) enters (or leaves) the correlator, there is no sample that can cancel the product to yield a zero output. In addition, the polyphase modulation of the CW carrier spreads the Power Spectral Density (PSD) out over a large bandwidth which is ideal for LPI radar.

Frequency modulation or Frequency Shift Keying (FSK) of a CW carrier signal can also be a useful LPI radar technique. A LPI radar that uses FSK techniques changes the transmitting frequency in time over a wide bandwidth in order to prevent an unintended receiver from intercepting the waveform. The frequency slots used are chosen from a frequency hopping sequence, and it is this unknown sequence that gives the radar the advantage in processing gain. That is, the frequency appears random to the intercept receiver and so the possibility of it following the changes in frequency is remote. As such, the FSK of a CW carrier is an LPI technique. This prevents a jammer from reactively jamming the transmitted frequency. Rapidly changing the transmitter frequency however, does not lower the PSD of the emission, but instead moves the PSD about according to the FSK sequence. Consequently the FSK radar is an LPI technique but not a Low Probability of Detection (LPD) technique. The most important FSK technique is the Costas sequence of frequencies. These frequencies produce unambiguous range and Doppler measurements while minimizing the cross talk between frequencies [4]. In general, the Costas sequence of frequencies provides an FSK code that produces peak sidelobes in the PAF that are down from the mainlobe response by a factor inversely proportional to the number of transmitted continuous frequencies. That is, the order of

frequencies in a Costas sequence or array is chosen in a manner to preserve an ambiguity response with a thumbtack nature (the narrow mainlobe and sidelobes are as low as possible) [1].

In order to spread the PSD of an FSK signal over a large bandwidth, the recent concept of a hybrid waveform has been introduced. In this waveform, the PSD of a FSK sequence is phase modulated by a polyphase waveform. Although phase codes such as the Frank code and the P4 code have been used, the recent development of complementary phase sequences to phase modulate the FSK waveform have not been studied. This type of signaling can achieve a high time-bandwidth product and can enhance the LPI/LPD features of the emitter waveform beyond that of each waveform individually. Periodic autocorrelation and ambiguity analysis of the signals reveal a lower Doppler- and time- (range) sidelobes and a lower integrated sidelobe level (ISL). The FSK/PSK techniques can also maintain a high Doppler tolerance, while yielding an instantaneous spreading the component frequencies along with an enhanced range resolution [5], [6].

B. PRINCIPAL CONTRIBUTIONS

To improve the range (time) sidelobe behavior, this thesis develops a new class of hybrid PSK/FSK CW signals for LPI/LPD radar applications. Three complementary sequences are used to phase modulate a Costas FSK waveform. Complementary sequences are those in which the sum of the PACFs of the sequences in that set is zero except for a zero-shift term. An example using a Frank polyphase code is first evaluated.

References that document recent advances in these sequence constructs were obtained and studied. The sequence values were coded in MATLAB and used to modulate a CW FSK waveform consisting of $f_j = \{3,2,6,4,5,1\}$ kHz frequencies. The new PSK/FSK waveforms are presented and the periodic ambiguity properties are evaluated. The PSK/FSK complementary sequences include the Golay Complementary Sequence (GCS) [7], the Quaternary Periodic Complementary Sequence (QPCS) [8], and the Quaternary Golay Complementary Sequence (QGCS) sequence [9]. The PACF and the PAF are evaluated for each hybrid waveform in order to quantify the range (time)

offset and Doppler offset sidelobe performance. The scope of the study is focused on providing an analysis of the results to identify the improvements in peak sidelobe performances and reduction of Doppler sidelobes. The new emitter architecture and signal processing algorithm is presented. The PACF and the PAF are evaluated for each waveform in order to quantify the range (time) offset and Doppler offset sidelobe performance.

C. THESIS OUTLINE

This thesis research, analysis, procedures, and results are organized in the following manner:

Chapter II provides a short description of radio frequency sensors that use LPI techniques. These include the antenna and transmitter characteristics of a LPI radar, the PSK and FSK signaling techniques and the hybrid PSK/FSK approach for these waveforms. Also described are the PACF and the PAF.

Chapter III presents the GCS as a technique to phase modulated the Costas FSK CW waveform to improve the time sidelobe behavior of received radar signals. Results presented include the ACF, PACF, and PAF.

Chapter IV describes a new construction method of QPCS proposed by Jang Ji-Woong et al., as a new technique to phase modulated the Costas FSK CW waveform to improve the time sidelobe behavior of received radar signals. Results presented include the ACF, PACF, and PAF.

Chapter V introduces the application of a new QGCS sets proposed by Zeng et al., as a new technique to phase modulated the Costas FSK CW waveform to improve the time sidelobe behavior of received radar signals, following the same analysis conducted in Chapters III and IV, in order to compare its differences and results.

Finally, concluding remarks are summarized in Chapter VI presenting an analysis of the results and a comparison between the three different techniques. Future works and its applicability in LPI radar technology are also presented.

II. RADIO FREQUENCY SENSOR

A. LPI RADAR

Many users today radar today are specifying a LPI and low probability of identification (LPID) as an important tactical requirement. The term LPI is that property of a radar that, because of its low power, wide bandwidth, frequency variability, or other design attributes, makes it difficult for it to be detected by means of a passive intercept receiver. A LPI radar is defined as a radar that uses a special emitted waveform intended to prevent a non-cooperative intercept receiver from intercepting and detecting its emission but if intercepted, makes identification of the emitted waveform modulation and its parameters difficult [1]. It follows that the LPI radar attempts detection of targets at longer ranges than the intercept receiver can accomplish detection/jamming of the radar. The success of an LPI radar is measured by how hard it is for the intercept receiver to detect/intercept the radar emissions.

The LPI requirement is in response to the increase in capability in modern intercept receivers to detect and locate a radar emitter [2]. One thing is for certain. For every improvement in LPI radar, improvements for intercept receiver design can be expected. In applications such as altimeters, tactical airborne targeting, surveillance, and navigation, the interception of the radar transmission can quickly lead to EA or jamming if the parameters of the emitter can be determined. Due to the wideband nature of these pulse compression waveforms, however, this is typically a difficult task. NOTE: we have extended the pulse compression term to CW modulations since the techniques are similar and the objective is the same. The LPI requirement is also in response to the ever-present threat of being destroyed by precision guided munitions and antiradiation missiles (ARMs). ARMs are designated to home in on active, ground-based, airborne or shipboard radars, and disable them by destroying their antenna systems and/or killing or wounding their operator crews [2].

The denial of signal intercept protects the emitters from most of these types of threats and is the objective of using a LPI waveform. Since LPI radar tries to use signals

that are difficult to intercept and/or identify, they have different design characteristics compared to conventional radar systems. These characteristics are discussed below.

1. Characteristics of LPI Radar

Many combine features helps the LPI radar prevent its detection by modern intercept receivers. These features are centered on the antenna (antenna pattern and scan patterns) and the transmitter (radiated waveform).

a. Antenna Considerations

The antenna is the interface, or connecting link between some guiding system and (usually) free space. Its function is to either radiate electromagnetic energy (the transmitter feed the guiding system) or receive electromagnetic energy (the guiding system feed the receiver system). The antenna pattern is the electric field radiated as a function of the angle measured from boresight (center of the beam). The various parts of the radiation pattern are referred to as lobes that may be subclassified into main, side, and back lobes [10]. The main lobe is defined as the lobe containing the direction of maximum radiation. The side lobe is a radiation lobe in any direction other than the intended lobe, and it represents the main focus of this study. A back lobe refers to a lobe that occupies the hemisphere in a direction opposite to that of the main lobe. The side lobe level is usually expressed as a ratio of the power density in the lobe in question to that of the main lobe. That is, the side lobe level is amplitude of the side lobe normalized to the main beam peak. The highest side lobe is usually that lobe closest to the main beam. It is also convenient to use the side lobe ratio (SLR), which is the inverse of the side lobe level [1].

b. Transmitter Considerations

A conventional radar that uses coherent pulse train has independent control of both range and Doppler resolution. This type of radar waveform also exhibits a range window that can be inherently free of side lobes. The main drawback of a coherent pulse train waveform is the high peak-to-average power ratio put out by the transmitter. The average power is what determines the detection characteristics of the radar. For high

average power, a short pulse (high range resolution) transmitter must have a high peak power, necessitating vacuum tubes and high voltages. The high peak power transmissions can also easily be detected by noncooperative intercept receivers. The duty cycle d_c for a pulse emitter relates the average transmitted power P_{avg} to the peak power P_t as

$$d_c = \frac{P_{avg}}{P_t} \tag{1}$$

The duty cycle can also be calculated as

$$d_c = \frac{\tau_R}{T_R} \tag{2}$$

where T_R is the pulse repetition interval (PRI – time between pulses) and τ_R is the emitter's pulse width or duration (in seconds). Typical duty cycles are $d_c = 0.001$ (the average power 0.001 times the peak power) for navigation radar.

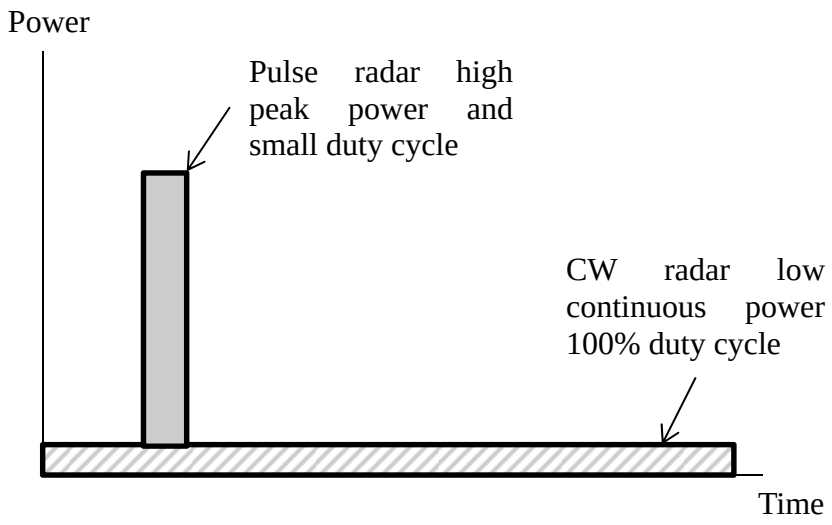

Figure 1. Comparison of a pulse radar and a CW radar. From [1].

In modulated CW signals, however, the average-to-peak power ratio is 1 or 100% duty cycle. This allows a considerably lower transmit power to maintain the same detection performance as the coherent pulse train radar. Also, solid state transmitters can be used that are lighter in weight. A comparison of a coherent pulse train

radar and the CW radar is shown in Figure 2. The CW radar has a low continuous power compared to the high peak power of the pulse radar but both can give the same detection performance. On the other hand, the final peak power for a pulsed system may be only a few decibels (dB) higher than the CW systems having equivalent performance.

Consequently, most LPI emitters use continuous wave (CW) signals. A CW (tone) signal is easily detected with a narrowband receiver and cannot resolve targets in range. LPI radars use periodically modulated CW signals resulting in large bandwidths and small resolution cells, and are ideally suited for pulse compression.

There are many pulse compression modulation techniques available that provide a wideband LPI CW transmit waveform. Any change in the radar's signature can help confuse an intercept receiver and make intercept difficult. The wide bandwidth makes the interception of the signal more difficult. For the intercept receiver to demodulate the waveform, the particular modulation technique used must be known (which is typically not the case). Pulse compression (wideband) CW modulation techniques include:

- Linear, nonlinear frequency modulation;
- Phase modulation (phase shift keying PSK);
- Frequency hopping (frequency shift keying FSK), Costas array;
- Combined (hybrid) phase modulation and frequency hopping (PSK/FSK);
- Noise modulation

With the above modulation techniques, the radiated energy is spread over a wide frequency range in a matter that is initially unknown to a hostile receiver. The phase and frequency modulation are not inherently wideband or narrowband. In this thesis, we are concerned with Costas FSK/PSK where we investigate the use of complementary sequences to phase modulate the carriers.

c. Carrier Frequency Considerations

Another LPI radar technique is choosing the emitter frequency strategically. The use of high operating frequency band that is within atmospheric

absorption lines makes interception difficult, but also makes the target detection by the radar even more difficult in most cases. Peak absorption occurs at frequencies of 22, 60, 118, 183, and 320 GHz [1]. The RF frequency can be chosen at these frequencies to maximize the attenuation in order to mask the transmit signal and limit reception by a hostile receiver (atmospheric attenuation shielding). Since the physics of radar detection, however, depends only on the energy placed on the target, LPI radar must still radiate sufficient effective radiate power (ERP) to accomplish detection. The loss for the radar due to atmospheric absorption is over its total two-way path (out to the target and back), while the interceptor's loss is over the one-way path (from the radar to the intercept receiver). Because of the high absorption of the emitter's energy, this technique is always limited to short range systems. For our study, we are using Costas FSK frequency hopping waveforms over a relatively large bandwidth.

In summary, the transmitter uses wideband modulation techniques (for the range resolution desired). Hybrid PSK/FSK waveforms along with the strategic selection of frequencies for a frequency hopping FSK waveform is of interest in this thesis. Most typically is that of a Costas frequency set [1]. By taking these characteristics into consideration the next section describes the importance of these hybrid radar waveforms.

B. AMBIGUITY ANALYSIS OF LPI WAVEFORMS

The ambiguity (delay-Doppler) analysis of LPI waveforms is important to understand the properties of the CW waveform and its effect on measurement accuracy, target resolution, ambiguity in range, and radial velocity, and its response to clutter [1].

1. The Ambiguity Function

A matched radar receiver performs a cross-correlation of the received signal and a reference signal, whose envelope is the complex conjugate of the envelope of the transmitted signal. The ambiguity function describes the response of a matched receiver to a finite duration signal. In ambiguity analysis, the receiver is considered matched to a target signal at a given delay and transmitted frequency. The ambiguity is then a function

of any added delay and additional Doppler shift from what the receiver was matched to. If $u(t)$ is the complex envelope of both the transmitted signal and the received signal, the ambiguity function is given by [11]

$$\left|\chi_{NT}(\tau,\nu)\right| = \left|\int_{-\infty}^{\infty} u(t)u^*(t-\tau)e^{j2\pi\nu t}dt\right| \tag{3}$$

where τ is the time delay and ν is the Doppler frequency shift. The 3D plot, as a function of τ and ν is called the ambiguity diagram. The maximum of the ambiguity function occurs at the origin $(\tau = 0, \nu = 0)$, and $\left|\chi(0,0)\right|$ is the output if the target appears at the delay and Doppler shift for which the filter was matched. The delay-Doppler response of the matched filter output is important for understanding the properties of the radar waveform [12]. Ideally, the ambiguity diagram would consist of a diagonal ridge centered at the origin, and zero elsewhere (no ambiguities). The ideal ambiguity function, however, is impossible to obtain. For a coherent pulse train consisting of N_R pulses with pulse duration τ_R and pulse repetition interval (PRI) T_r, the ambiguity function indicates that the Doppler resolution is the inverse of the total duration of the signal $N_R T_r$ while the delay resolution is the pulse duration [13].

2. Periodic Autocorrelation Function (PACF)

LPI signals are typically low-power CW waveforms that are modulated by a periodic function, such as the phase code sequence or linear frequency ramp. A major advantage of the periodically modulated CW waveform is that they can yield a perfect PACF [1]. For example, consider a phase-coded CW signal with N_c phase codes each with subcode duration t_b s. The transmitted CW signal has a code period $T = N_c t_b$ and a periodic complex envelope $u(t)$ given as

$$u(t) = u(t + nT) \tag{4}$$

for $n = 0, \pm 1, \pm 2, \pm 3....$ The values of the PACF as a function of the delay r (which are multiples of t_b) are given by

$$R(rt_b) = \frac{1}{N_c}\sum_{n=1}^{N_c} u(n)u^*(n+r) \tag{5}$$

and ideally we would like a perfect PACF or

$$R(rt_b) = \begin{cases} 1, & r=0 \pmod{N_c} \\ 0, & r\neq 0 \pmod{N_c} \end{cases} \tag{6}$$

Since the CW signal is continuous, the perfect PACF is possible.

3. Periodic Ambiguity Function (PAF)

The periodic ambiguity function describes the response of a correlation receiver to a CW signal modulated by a periodic waveform with period *T*, when the reference signal is constructed from an integral number *N* of periods of the transmitted signal (coherent processor length *NT*) [14]. The target illumination time (dwell time) *PT* must be longer than *NT*. As long as the delay τ is shorter than the difference between the dwell time and the length of the reference signal $0 \le \tau \le (P-N)T$, the illumination time can be considered infinitely long and the receiver response can be described by the PAF given as [15]

$$\left|\chi_{NT}(\tau,\nu)\right| = \left|\frac{1}{NT}\int_0^{NT} u(t-\tau)u^*(t)e^{j2\pi\nu t}dt\right| \tag{7}$$

where τ is assume to be constant, and the delay rate of change is represented by the Doppler shift ν. The PAF for *N* periods is related to the single-period ambiguity function by a universal relationship

$$\left|\chi_{NT}(\tau,\nu)\right| = \left|\chi_T(\tau,\nu)\right|\left|\frac{\sin(N\pi\nu T)}{N\sin(\pi\nu T)}\right| \tag{8}$$

where

$$\left|\chi_{NT}(\tau,\nu)\right| = \frac{1}{T}\left|\int_0^{T} u(t-\tau)u^*(t)e^{j2\pi\nu t}dt\right| \tag{9}$$

is the single PAF. The single PAF is multiply by a universal function of *N* and *T* that is independent of the complex envelope of the signal and that does not change with τ. The PAF shows the effect of using a reference receiver consisting of *N* code periods and examining Equation (8) reveals that for a large number of code periods *N*, the PAF is increasingly attenuated for all values of ν except at multiples of $1/T$. It also have main lobes at $\nu T = 0, \pm 1, \pm 2, \ldots$. Equation (8) also reveals that the PAF has relatively strong

Doppler side lobes. Matter that will be take into consideration for the analysis in order to determine its differences in the time sidelobes levels between the different complementary sequences that will be implemented.

The PAF serves CW radar signals in a similar role to which the traditional ambiguity function serves finite duration signals. Note that for a large *N*, the PAF is compressed to zero for all ν, except near $\nu = n/T, n = 0, \pm 1, \pm 2, \ldots$. For an infinitely large *N*, the function $\left|\chi_{NT}(\tau,\nu)\right|$ becomes a train of impulses. For large *N*, the PAF of a sequence exhibiting perfect periodic autocorrelation will strongly resemble the ambiguity function of a coherent pulse train [1].

a. Periodicity of the PAF

The PAF formulation given in (9) represents the straightforward implementation of the matched filter to the signal $u(t)$ delayed by τ and Doppler shift by ν. It can easily be shown that the cut along the PAF's delay axis $\left|\chi_{NT}(\tau,0)\right|$ (zero Doppler) is the magnitude of the PACF of the signal given by (7) [14]. The cut along the Doppler axis (zero delay) is

$$\chi_{NT}(0,\nu) = \frac{1}{NT}\int_0^{NT} \left|u(t)\right|^2 e^{j2\pi\nu t} dt \tag{10}$$

Assuming a constant amplitude signal, $\left|u(t)\right| = 1$ (e.g., phase-modulated CW signals)

$$\left|\chi_{NT}(0,\nu)\right| = \left|\frac{\sin(\pi\nu NT)}{\pi\nu NT}\right| \tag{11}$$

and

$$\left|\chi_{NT}(0,0)\right| = 1 \tag{12}$$

For any integer *n*, the periodicity on the delay axis is

$$\left|\chi_{NT}(nT,\nu)\right| = \left|\chi_{NT}(0,\nu)\right| \tag{13}$$

For the ν axis, for $m = 0, \pm 1, \pm 2, \ldots$

$$\left|\chi_{NT}(\tau, m/T)\right| = \left|\chi_{NT}(\tau + nT, m/T)\right| \tag{14}$$

The symmetry cuts are a function of the three parameters: the code period *N*, the number of phase codes N_c, and the number of code periods used in the correlation receiver *N*.

4. Peak and Integrated Side Lobe Levels

The time side lobes level in the ACF help quantify the LPI waveforms in its ability to detect targets without interfering side lobe targets. That is, if the ACF has high side lobes, a second nearby target might be able to hide in a side lobe and go undetected. To quantify the LPI waveform characteristics, the peak side lobe level (PSL) of the ACF can be defined as

$$PSL = 10\log_{10}\left[\frac{\text{max side lobe power}}{\left(\text{peak response}\right)^2}\right] = 10\log\left[\frac{\max\ \mathrm{R}^2(k)}{R^2(0)}\right] \tag{15}$$

where k is the index for the points in the ACF, $R(k)$ is the ACF for all of the output range side lobes except that at k=0, and $R(0)$ is the peak of the ACF at k = 0. The integrated side lobe level (ISL) is

$$ISL = 10\log_{10}\left[\frac{\text{total power in side lobes}}{\left(\text{peak response}\right)^2}\right] = 10\log\sum_{k=-M}^{M}\frac{R^2(k)}{R^2(0)} \tag{16}$$

and is a measure of the total power in the sidelobes as compared with the compressed peak. The PSL is a useful measure when a single point target response is of concern. Values of the PSL depend on the number of subcodes in the code sequence N_c as well as the number of code periods N within the receiver. The ISL is considered a more useful measure than the PSL when distributed targets are of concern. Typical matched filter ISL values range from -10 to -20 dB [1].

5. Properties of the ACF, PACF, and PAF

To demonstrate the properties of the ACF, PACF, and PAF, we look briefly as an example at the Frank code, considering its variable length and that it can be used to phase modulate a complex signal every subcode period t_b.

The transmitted signal can be written as

$$s(t) = \Re\left\{Ae^{(j2\pi f_c t+\phi_k)}\right\} \tag{17}$$

where f_c is the carrier frequency and ϕ_k is the phase modulation that is used to shift the phase of the carrier in time every subcode period according to the particular phase

modulation used. Note that the carrier frequency remains constant. The Frank phase modulation code is derived from a step approximation to a linear frequency modulation wavefrom using *M* frequency steps and *M* samples per frequency. If *i* is the number of the sample in a given frequency and *j* is the number of the frequency, the phase of the *i*th sample of the *j*th frequency for the Frank code is

$$\phi_{i,j} = \frac{2\pi}{M}(i-1)(j-1) \tag{18}$$

where $i = 1,2,\ldots,M$, and $j = 1,2,\ldots,M$. The Frank code has a length of $N_c = M^2$ subcodes, which is also the corresponding pulse compression ratio or processing gain PG_R. For t_b s (the subcode period), the cpp represents the number of carrier cycles per subcode, then $t_b = cpp/f_c$ s resulting in a transmitted signal bandwidth $B = 1/t_b = 1/cpp$. The code period can also be expressed as

$$T = N_c t_b = M^2 t_b \tag{19}$$

Figure 2 shows the Frank phase modulation (52) with $M = 8$ $(N_c = 64)$ where the carrier frequency is $f_c = 1$ kHz, $f_s = 7$ kHz, and cpp=1. Figure 3 shows the power spectral density of the frank signal. Note that since the cpp=1, the 3-dB bandwidth $B = 1$ kHz, as illustrated.

The ACF and the PACF are shown in Figure 4 for the number of code periods $N = 1$. These results are obtained by using the LPI toolbox (LPIT) developed in [1] with $r = 1$, $F * Mt_b = 10$, $T = 1$, $N = K = 100$. The PSL can be read from Figure 4(a). The largest side lobe level is 28 dB down from the peak. This is in agreement with the theoretical result $PSL = 20\log_{10}(1/M\pi) = -28$ dB (voltage ratio). Also note form Figure 4(b) that the CW Frank signal has a perfect PACF (zero side lobes). The PAF for $N = 1$ is shown in Figure 5. The phase modulation signals generated using the LPIT contain

$$b_{sc} = \frac{cpp \cdot f_s}{f_c} \tag{20}$$

number of samples per subcode. The total number of samples within a code period is then $N_c b_{sc}$.

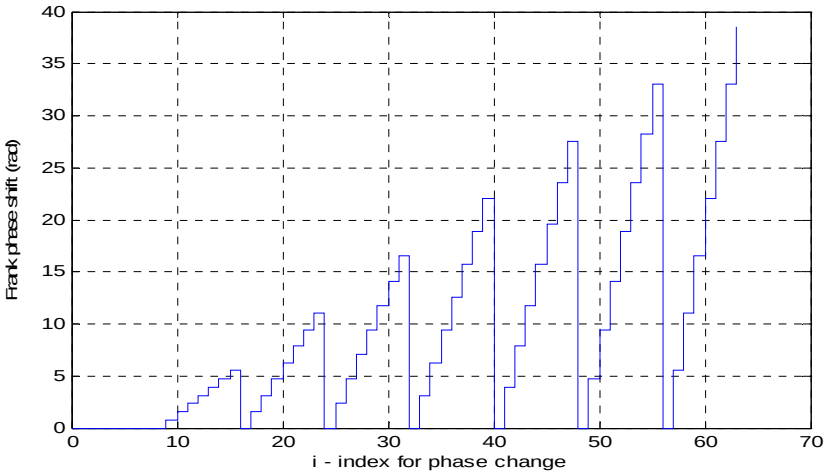

Figure 2. Frank phase modulation for $M = 8$ $(N_c = 64)$.

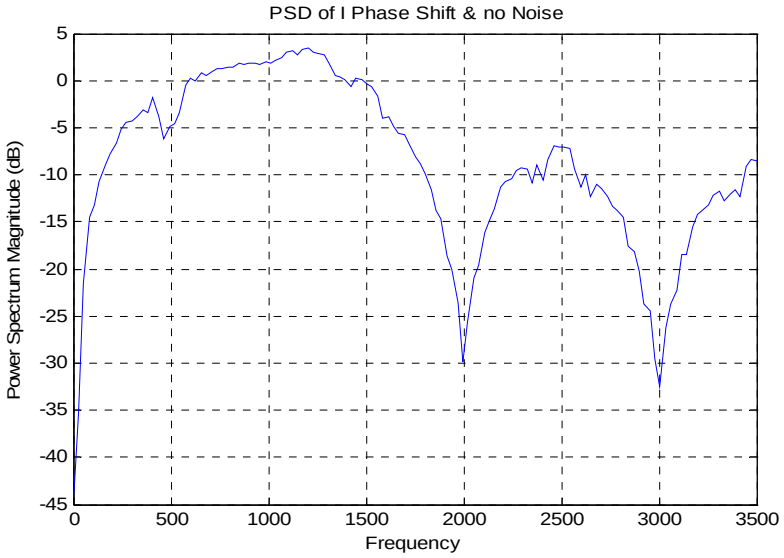

Figure 3. Power spectral density for Frank phase modulation.

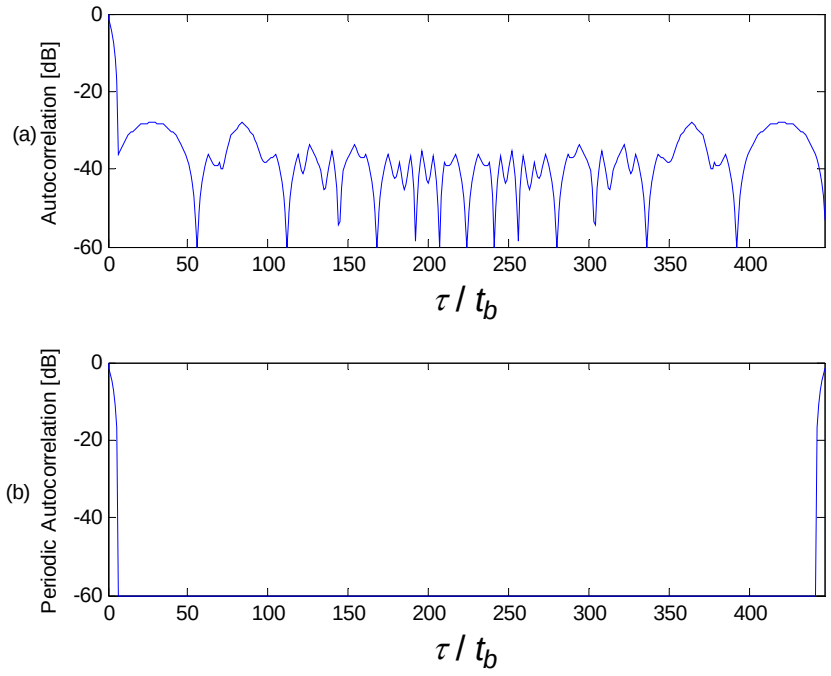

Figure 4. Frank (a) ACF (PSL= -28 dB down) and (b) PACF for $M = 8$, cpp=1 with number of reference waveforms $N = 1$.

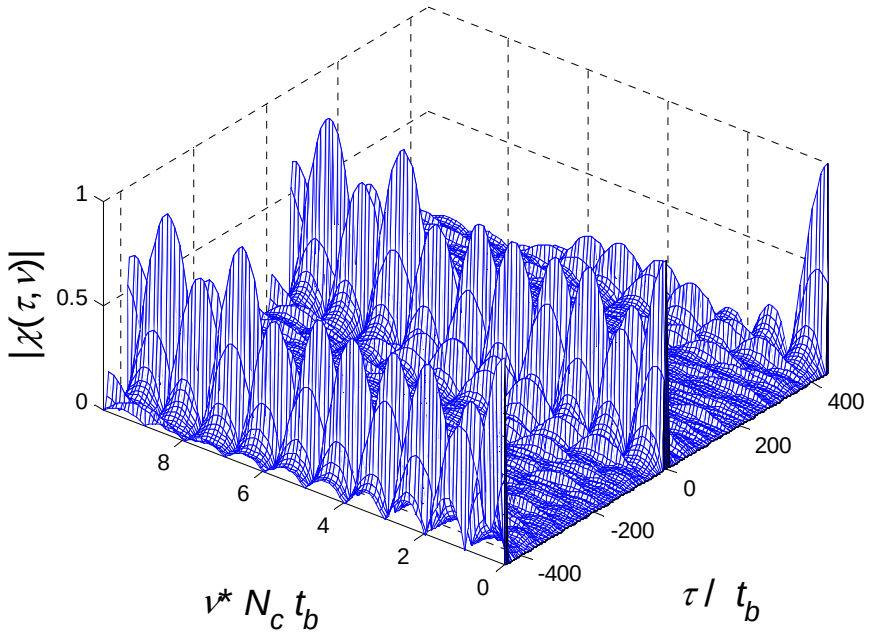

Figure 5. PAF for Frank phase modulation for $M = 8$ $(N_c = 64)$, $cpp = 1$ with number of reference waveforms $N = 1$.

Increasing the number of code periods N used in the receiver can help to decrease the Doppler side lobes as well as the time side lobes in the ACF. Figure 6 shows the ACF and PACF for when N = 4 code periods are used within the reference receiver $(r=1, F*Mt_b=40, T=0.3, N=K=100)$. Including N in the estimation of the peak side lobe level

$$PSL = 20\log_{10}\left(\frac{1}{NM\pi}\right)dB \tag{21}$$

Using N = 4, PSL = -40dB down from the peak shown in Figure 6(a).

Figure 7 shows the PAF of the Frank code with N = 4 and demonstrates that by using more copies of the reference signal within the correlation receiver, the delay-Doppler side lobe performance improves, important consideration take into account for the analysis by applying it among the different complementary sequences implemented.

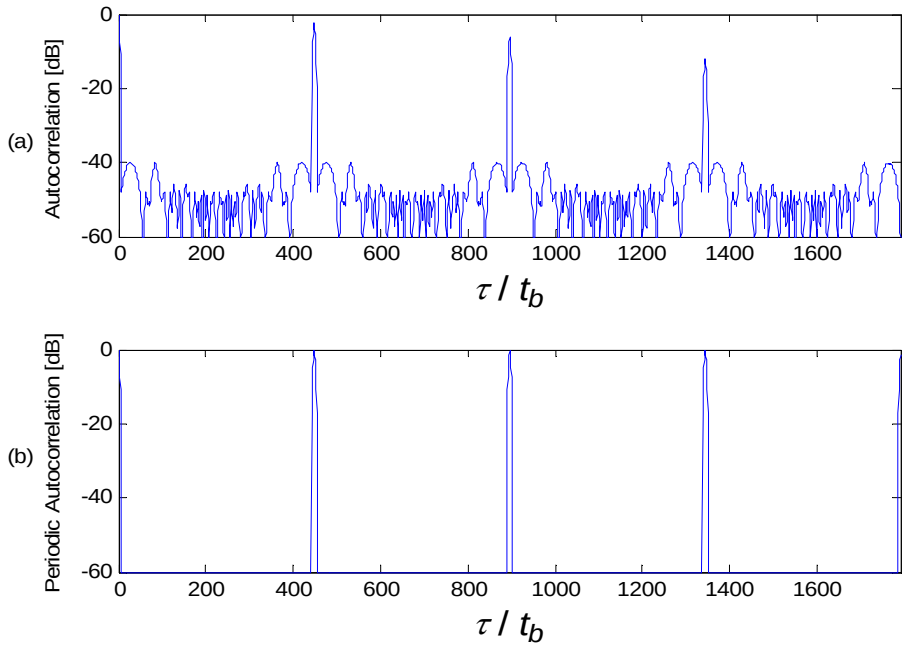

Figure 6. Frank (a) ACF (PSL = -40 dB down) and (b) PACF for M = 8 (N_c = 64), *cpp* = 1 with number of reference N = 4.

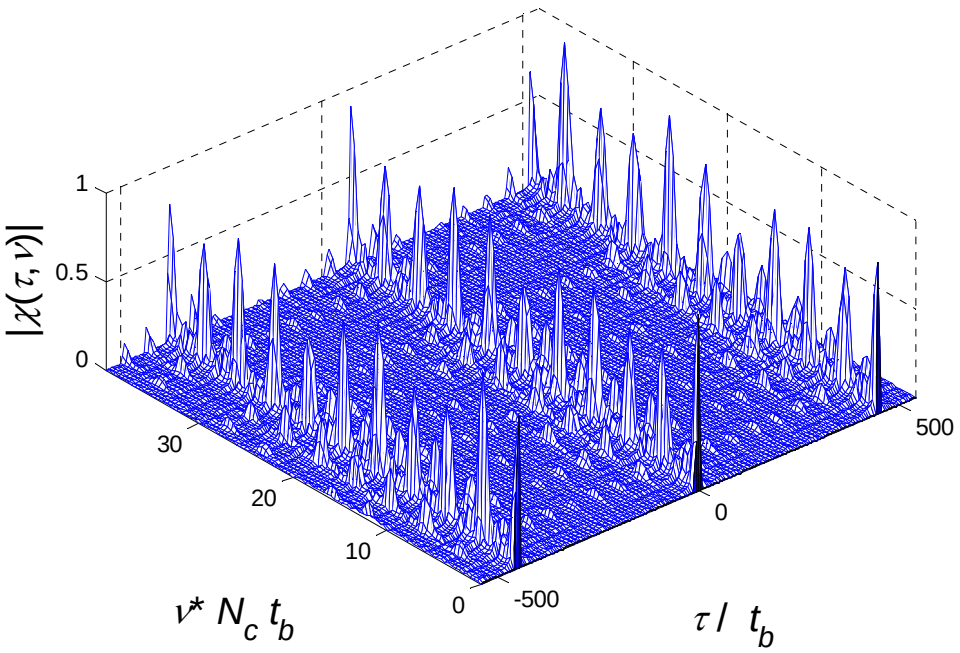

Figure 7. PAF for Frank phase modulation for $M = 8\,(N_c = 64)$, $cpp = 1$ with number of reference waveforms $N = 4$.

From Figure 7 it can also be noted that the Delay and the DSL are much lower than the BPSK signal examined in II.

To develop the comparison between the three different complementary sequences described in Chapter I, a CW Costas six-frequency waveform is used for each code period. Each frequency is divided into sub-codes and with duration of each sub-code of $t_p = 7$ ms. For each waveform five code periods are generated providing a working example as well as to give capability to evaluate the three different complementary sequence sets. Results of the PSL, ISL, and PDS are obtained by following the steps established in the flow chart from Figure 8. The results are shown and then analyzed in Chapter VI.

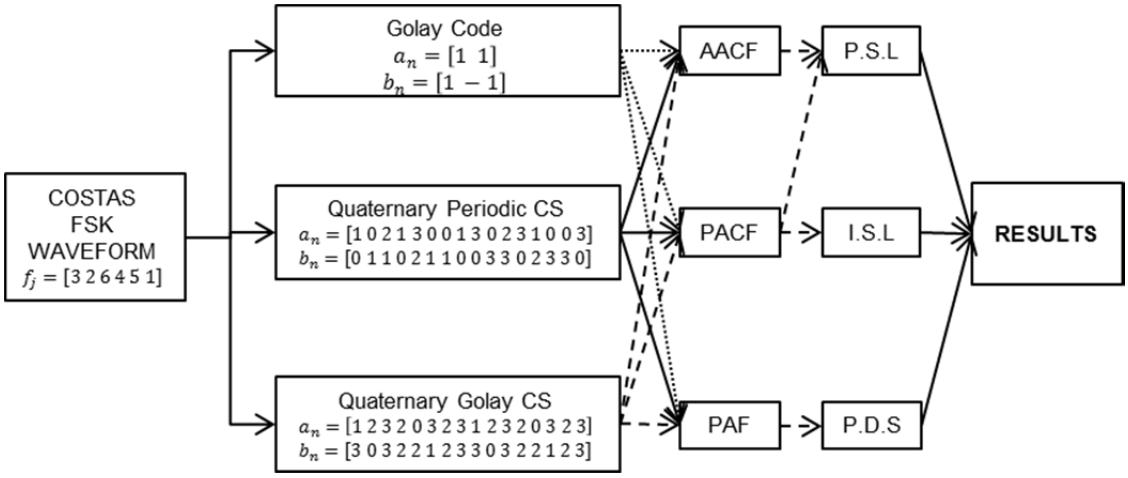

Figure 8. Analysis' process flow chart.

In the next chapter, details on the use of Golay complementary sequences to encode Costas FSK CW waveforms in order to improve the range (time) sidelobe behavior are presented by applying the techniques above described.

C. LPI RADAR WAVEFORM

The hybrid LPI radar technique combines the technique of FSK (FH using Costas sequences) with that of the PSK modulation using sequences of varying length [5], [6]. This type of signaling can achieve a high time-bandwidth product of processing gain, enhancing the LPI features of the radar. Ambiguity properties of the signal are retained by preserving the desirable properties of the separate FSK and PSK signaling schemes. The FSK/PSK techniques can maintain a high Doppler tolerance, while yielding an instantaneous spreading of the component frequencies along with an enhance range resolution [5]. Below, FSK and PSK signals are described.

1. Phase Shift Keying (PSK)

While linear Frequency Modulation CW (FMCW) has established itself as one of the most popular LPI waveforms, PSK CW waveforms have recently been a topic of active investigation, due to their wide bandwidth and inherently low Periodic Ambiguity Function (PAF) side lobe levels achievable. For the LPI radar (as with pulse radar), it is important to have a low side lobe level to avoid the side lobes of large targets from

masking the main peak of smaller targets. The choice of PSK codes affects the radar performance and the implementation. For the PSK waveforms, the bandwidth (inverse of the subcode period) is selected first by the designer, in order to achieve the range resolution desired. Encompassing a large target (such as a ship) within a single resolution cell can aid in detection, but results in a narrow bandwidth signal. On the other hand, a wideband transmitted signal can be chosen to divide the target echo into many resolution cells, and is a technique that is useful for target recognition. The trade-off here is that the radar requires a larger transmitted power to detect a target that has a small cross section, decreasing the ability of the radar to remain quiet [1].

Binary phase shift codes (e.g., 0 to 180 degrees) are popular, but provide little in the way of low side lobes and Doppler tolerance. Most useful for the LPI radar are the polyphase codes where the phase shift value within the subcode can take on many values (not just two) and the code period T can be made extremely long. These codes have better sidelobe performance and better Doppler tolerance than the binary phase codes.

The PSK technique can result in a high range resolution waveform, while also providing a large SNR processing gain for the radar. The average power of the CW transmission is responsible for extending the maximum detection range while improving the probability of target detection (as compared to a pulsed signal of equal peak power). PSK techniques are also compatible with new digital signal processing hardware, and a variety of side lobe suppression methods [16] can be applied. Compatibility with solid state transmitters enables power management of the transmitted CW signal. Power management allows the radar to keep a target's SNR constant within the receiver, as the range to the target changes.

a. The Transmitted Signal

In a PSK radar, the phase shifting operation is performed in the radar's transmitter, with the timing information generated from the receiver-exciter. The transmitted complex signal can be written as

$$s(t) = Ae^{j(2\pi f_c t + \phi_k)} \tag{22}$$

where ϕ_k is the phase modulation function that is shifted in time, according to the type of PSK code being used, and the f_c is the angular frequency of the carrier. The inphase (I) and quadrature (Q) representing the complex signal from the transmitter can be represented as

$$I = A\cos(2\pi f_c t + \phi_k) \tag{23}$$

and

$$Q = A\sin(2\pi f_c t + \phi_k) \tag{24}$$

Within a single code period, the CW signal is phase shifted N_c times, with phase ϕ_k every t_b seconds, according to a specific code sequence. Here t_b is the subcode period. The resulting code period is

$$T = N_c t_b \quad s \tag{25}$$

And the code rate is

$$R_c = 1/N_c t_b \quad s^{-1} \tag{26}$$

The transmitted signal can be expressed as

$$u_T = \sum_{k=1}^{N_c} u_k[t-(k-1)t_b] \tag{27}$$

for $0 \le t \le T$ and zero elsewhere. The complex envelope u_k is

$$u_k = e^{j\phi_k} \tag{28}$$

for $0 \le t \le t_b$ and zero otherwise. The range resolution of the phase coding CW radar is

$$\Delta R = \frac{ct_b}{2} \tag{29}$$

and the unambiguous range is

$$R_u = \frac{cT}{2} = \frac{cN_c t_b}{2} \tag{30}$$

If cpp is the number of cycles of the carrier frequency per subcode, the bandwidth of the transmitted signal is

$$B = f_c/cpp = 1/t_b \quad Hz \tag{31}$$

The received waveform from the target is digitized and correlated in the receiver using a matched (unweighted) or mismatched (weighted) filter that contains a cascade of *N* sets

of N_c reference coefficients. The results from each correlation are combined to concentrate the target's energy and produce a compressed pulse having a time resolution equal to the subcode duration t_b and a height of N_c. For this reason, the number of phase code elements N_c is also called the compression ratio. Recall that the PAF describes the range-Doppler performance of this type of receiver, and depends on the number of reference sets used.

Because the choice of PSK code affects the radar performance and the implementation, below are the different types described.

b. Binary Phase Codes (Barker)

A Barker sequence is a finite sequence $A=\left[a_0,a_1,...,a_n\right]$ of +1's and -1's of length $n\geq 2$ such that the aperiodic autocorrelation coefficients (or side lobes) are

$$r_k=\sum_{j=1}^{n-k}a_j a_{j+k} \tag{32}$$

satisfies $\left|r_k\right|\leq 1$ for $k\neq 0$ and similarly $r_{-k}=r_k$.

Consequently, a binary Barker sequence has elements $a_i\in\left\{-1,+1\right\}$, which are only known for lengths $N_c=2,3,4,5,7,11,$ and 13. A list of the nine known Barker sequences is shown in Table 1.3 along with their Peak Sidelobe Level (PSL) and Integrated Sidelobe Level (ISL) in decibels. The nine sequences are listed where +1 is represented by a + and a -1 is represented by a -. Figure 2 shows the ACF $\left(r_k\right)$ and the PACF of a CW signal phase coded with an $N_c=13-$bit Barker sequence, and reveals the side lobe structure of the code. For the signal, $f_c=1$ kHz and the sampling frequency $f_s=7$ kHz. Note the sidelobe characteristics reflecting the perfect nature of the Barker codes. For the $N_c=13$-bit code shown, PSL$=20\log_{10}(1/N_c)=-22.3$ dB. The number of cycles per phase $cpp=1.$ The PACF plot reveals the fact that the Barker codes do not have perfect PACF side lobe characteristics (zero side lobes)), but have a lowest side lobe levels that equals the PSL shown for the AFC (-22 dB).

Code Length	Code Elements	PSL (dB)	ISL (dB)
2	−+, +−	–6.0	–3.0
3	++−	–9.5	–6.5
4	++−+	−12.0	–6.0
4	+++−	−12.0	–6.0
5	+++−+	−14.0	–8.0
7	+++−−+−	−16.9	–9.1
11	+++−−−+−−+−	–20.8	–10.8
13	+++++−−++−+−+	–22.3	−11.5

Table 1. Nine Barker Codes with corresponding PSL and ISL. From [1].

Upon reception of the target's return signal, the receiver uses a detector to generate a + or – for each subcode. Figure 9 demonstrates the binary phase coding technique and receiver architecture using an $N_c = 13$-bit Barker code. In this figure, the receiver output uses a single tapped delay line matched filter to compress the transmitted waveform. When the return signal vector is centered within the filter, the + filter coefficients line up with the signal +'s and – filter coefficients line up with signals –'s, and a maximum output results as shown.

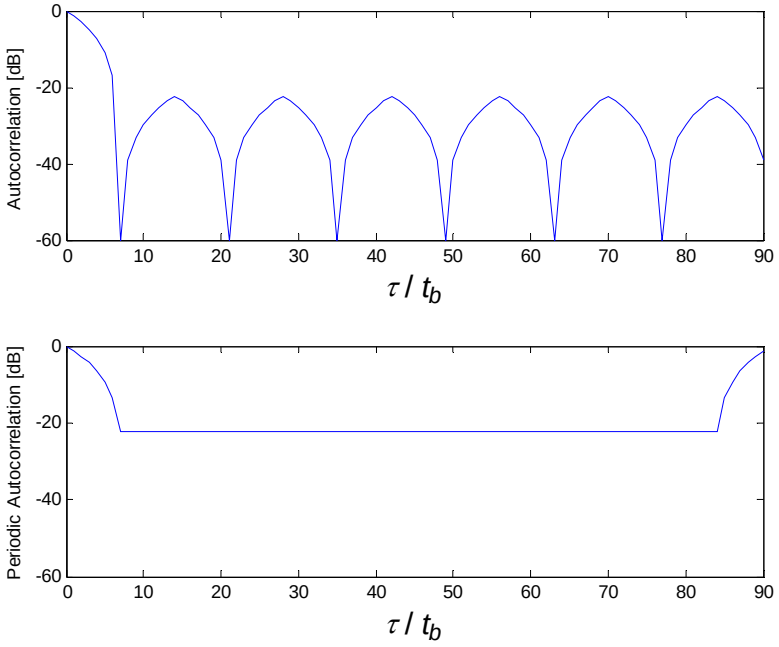

Figure 9. ACF and PACF for the $N_c = 13$-bit binary PSK signal. From [1].

c. Polyphase Codes

Polyphase sequences are finite length, discrete time complex sequences with constant magnitude but with a variable ϕ_k. Polyphase coding refers to phase modulation of the CW carrier, with a polyphase sequence consisting of a number of discrete phases. That is, the sequence elements are taken from an alphabet of size $N_c > 2$. Increasing the number of elements or phase values in the sequence allows the construction of longer sequences, resulting in a high range resolution waveforms with greater processing gain in the receiver or equivalently a larger compression ratio. The trade-off is that a more complex matched filter is required compare to a Barker code filter [1]. Figure 10 describes the binary phase coding techniques and receiver architecture scheme using a 13-Barker code.

The importance of polyphase coding in the LPI analysis is that by increasing the alphabet size N_c, the autocorrelation side lobes can be decreased significantly while providing a larger processing gain. By narrowing the subcode width

t_b (so there are fewer cycles per phase), the transmitted signal can also be spread over a large bandwidth, forcing the receiver to integrate over a larger band of frequencies.

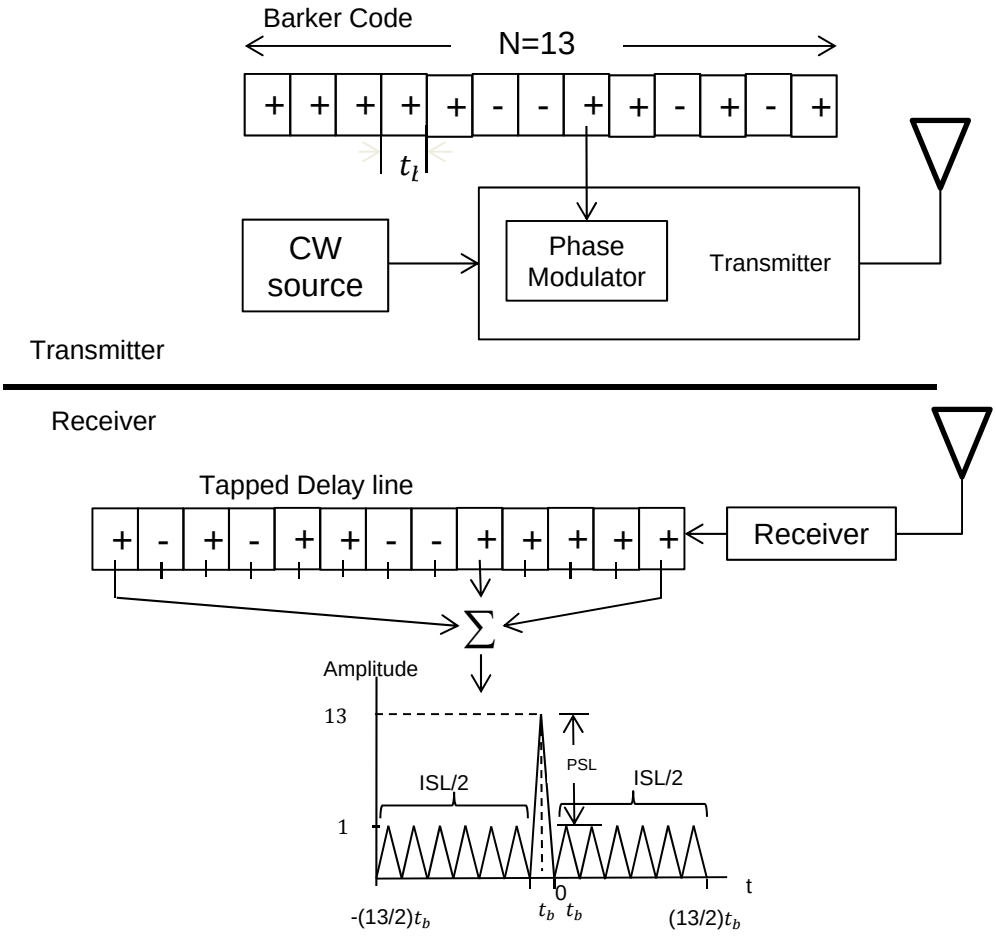

Figure 10. Binary phase coding techniques and receiver architecture using a 13-Barker code $\left(N_c = 13\right)$. After [1].

d. Polyphase Barker Code

Polyphase Barker codes allow the LPI emitter a larger amount of flexibility in generating the phase modulated waveforms. Since the number of different phase terms (or alphabet) is not two-valued, there is considerable advantage to their use since they are unknown to the nooncooperative intercept receiver.

Consider the generalized barker sequences $\{a_j\}$ of infinite length *n* where the terms a_j are allowed to be complex numbers of absolute value 1 where the correlation is now the Hermitian dot product[1]

$$r_k = \sum_{j=1}^{n-k} a_j a_{j+k}^* \tag{33}$$

where z^* represents the complex conjugate of z. A class of transformations can be developed that leave the absolute values of the correlation function unaltered, so that, in particular, generalized Barker sequences are changed into other generalized Barker sequences [17].

e. Frank Code

In 1963, R.L Frank devised a polyphase code that is closely related to the linear frequency modulation and Barker codes [18]. The Frank code is well documented and has recently been used successfully in LPI radars. The Frank code is derived from a step approximation to a linear frequency modulation waveform using *M* frequency steps and *M* samples per frequency. The Frank code has a length or processing gain of $N_c = M^2$ [19].

2. Frequency Shift Keying (FSK)

Coding technique that increases the library of LPI radar waveform and three important FSK or frequency hopping (FH) techniques for coding CW waveforms are described below.

An LPI radar that uses FH techniques hopes or changes the transmitting frequency in time over a wide bandwidth in order to prevent an unintended receiver from intercepting the waveform. The frequency slots used are chosen from an FH sequence, and it is this unknown sequence that gives that gives the radar the advantage in terms of processing gain. That is, the frequency sequence appears random to the intercept receiver, and so the possibility of it following the changes in frequency is remote. In contrast to the

[1] The Hermitian dot product of two vectors $(x_1, x_2, ..., x_n), (y_1, y_2, ..., y_n)$ is $\sum_{i=1}^{n} x_i y_i^*$.

FMCW and PSK techniques, the FH technique of rapidly changing the transmitter frequency does not lower the PSD of the emission, but instead moves the PSD about according to the FH sequence. Consequently, the FH radar has a higher probability of detection than the PSK or FMCW waveform, but retains a significantly low probability of interception.

a. The Transmitted Signal

In an FSK radar, the transmitted frequency f_j is chosen form the FH sequence $\left\{ f_1, f_2, ..., f_{N_F} \right\}$ of the available frequencies for transmission at a set of consecutive time intervals $\left\{ t_1, t_2, ..., t_{N_F} \right\}$. The frequencies are placed in the various time slots corresponding to the binary time-frequency matrix. Each frequency is used once within the code period, with one frequency per time slot and one time slot per frequency. The expression for the complex envelope of the transmitted CW FSK is given by

$$s(t) = Ae^{j2\pi f_j t} \tag{34}$$

The transmitted waveform has N_F contiguous frequencies within a band *B*, with each frequency lasting t_p s in duration.

CW FSK radars using multiple frequencies can compute very accurate range measurements. To illustrate, consider a CW radar that transmits the waveform

$$s(t) = A\sin(2\pi f_j t) \tag{35}$$

where the received signal from a target at a range R_T is

$$s(t) = A\sin(2\pi f_j t - \phi_T) = A\sin\left(2\pi f_j t - \frac{4\pi f_j R_T}{c} \right) \tag{36}$$

Since the range to the target depends on the frequency difference, the range resolution than depends on the duration of each frequency as

$$\Delta R = \frac{ct_p}{2} \tag{37}$$

The transmitted power for each frequency must be such that the energy content within the target echo is sufficient for detection, and enough to ensure that accurate phase measurements can be made.

In summary, for the FSK CW radar, the frequency difference Δf determines the maximum unambiguous detection range. The target's range computed by measuring the return signal phase difference from two consecutives transmitted frequencies. The range resolution, ΔR , depends only on the FH period [1].

b. Costas Codes

In a study by J.P Costas, techniques were presented for generating a sequence of frequencies that produce unambiguous range and Doppler measurements while minimizing the cross talk between frequencies [4]. In general, the Costas sequence of frequencies provides an FH code that produces peak side lobes in the PAF, that are down from the main lobe response by a factor of $1/N_F$ for all regions in the delay-Doppler frequency plane. That is, the order of frequencies in a Costas sequence or array us chosen in a manner to preserve an ambiguity response with a thumbtack nature (the narrow main lobe and side lobes are as low as possible). The firing order of these frequencies is based on primitive roots (elements) of finite fields.

A Costas array or (frequency) sequence $f_1, \ldots, f_{N_F}$ is a sequence that is permutation of the integers 1,…,N_F satisfying the property

$$f_{k+1} - f_k \neq f_{j+i} - f_j \tag{38}$$

for every i, j, and k such that $1 \leq k < i < i + j \leq N_F$. An array that results from a Costas sequence in this way is called a Costas array.

c. Costas Sequence PAF

The PAF can be approximate by overlaying the binary time-frequency matrix upon itself, and shifting one relative to the other according to a particular delay (horizontal shifts) and particular Doppler (vertical shifts). At each combination of shifts, the sum of coincidences between points of the fixes and the shifted matrix represents the

relative height of the PAF. The PAF is constructed by considering each row (delay) in the difference triangle, and placing a "1" in the PAF delay-Doppler cell corresponding to each $\Delta_{i,j}$.

d. Construction of Costas Arrays

There are many analytical procedures for constructing Costas frequency hopping arrays. Although Costas arrays may exist in principle for any positive integer N_F, these analytical construction methods are typically limited to values of N_F related to prime numbers [6], [8], [9]. Most construction methods to produce a large number of Costas arrays of equal length are based on the properties of primitive roots [1].

The most common method is the Welch, in which for the construction of a Costas array, an odd prime number *p* is chosen first. The number of frequencies and the number of time slots in the Costas sequence are then $N_F = \phi(p) = p - 1$ where $\phi(p)$ is the Euler function. Next, a primitive root *g* modulo *p* is chosen. Since *g* is a primitive root modulo $p, g, g^2, ..., g^{\phi(p)}$ are mutually incongruent and form a permuted sequence of the reduced residues *p*. Welch showed that this reduced residue sequence is a Costas sequence.

3. Hybrid FSK/PSK Emitter

The hybrid LPI radar technique combines the technology of FSK (FH using Costas sequences) with that of PSK modulation using varying length [5], [6]. This type of signaling can achieve a high time band-width product of processing gain, enhancing the LPI features of the radar. Ambiguity properties of the signal are retained by preserving the desirable properties of the separate FSK and PSK signaling schemes. The FSK/PSK techniques can maintain a high Doppler tolerance, while yielding an instantaneous spreading of the component frequencies along with an enhanced range resolution [5]. For purposes of this analysis, a Costas-based FSK/PSK signal (Barker 5-bit PSK over each frequency) is analyzed.

a. FSK/PSK Signal

Recall that for the FH LPI radar, the CW waveform has N_F contiguous frequencies within a bandwidth *B*, whit each frequency lasting t_p s in duration. The hybrid FSK/PSK signal further subdivides each subperiod into N_B phase slots, each of duration t_b as shown in Figure 11. The total number of phase slots in the FSK/PSK waveform is then

$$N_T = N_F N_B \tag{39}$$

with the total code period $T = t_b N_B N_F$. The expression for the complex envelope of the transmitted CW FSK/PSK signal is given by

$$s(t) = Ae^{j2\pi f_j t + \phi_k} \tag{40}$$

where ϕ_k is one of the N_B Barker codes for the analysis presented, and f_j is one of the N_F Costas frequencies [1].

During each hop, the signal frequency (one of the N_F frequencies) is modulated by a binary phase sequence, according to a Barker code sequence of length $N_B = 5$, 7, 11, or 13. In order to show the process, the FSK/PSK signal generated by using the $N_F = 16$ Costas sequence $f = \{3, 2, 6, 4, 5, 1\}$, and phase modulating it with a Barker binary phase modulation of length $N_B = 5$ gives a signal with a final waveform as a binary phase modulation within each frequency hop, resulting in five phase subcodes equally distributed within each frequency, for a total of $N_P N_F = 30$ subcodes.

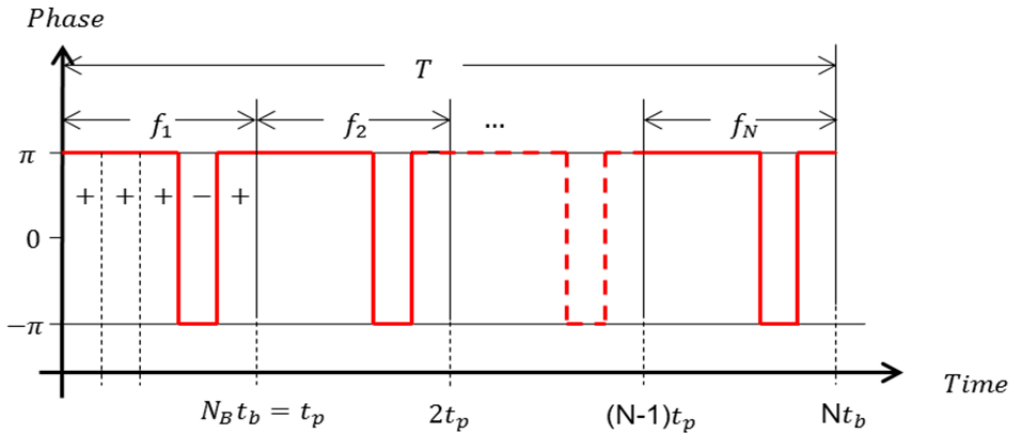

Figure 11. General FSK/PSK signal containing N_F frequency subcodes (hops) each with duration t_p s. Each frequency subcode is subdivided into N_B phase slots, each with duration t_b .

As an illustrative example, Figure 12 shows the CW waveform using a Frank Code with a 7 kHz sampling frequency, 1 kHz carrier frequency, 1 cycle per phase, 64 phase codes within 8 samples.

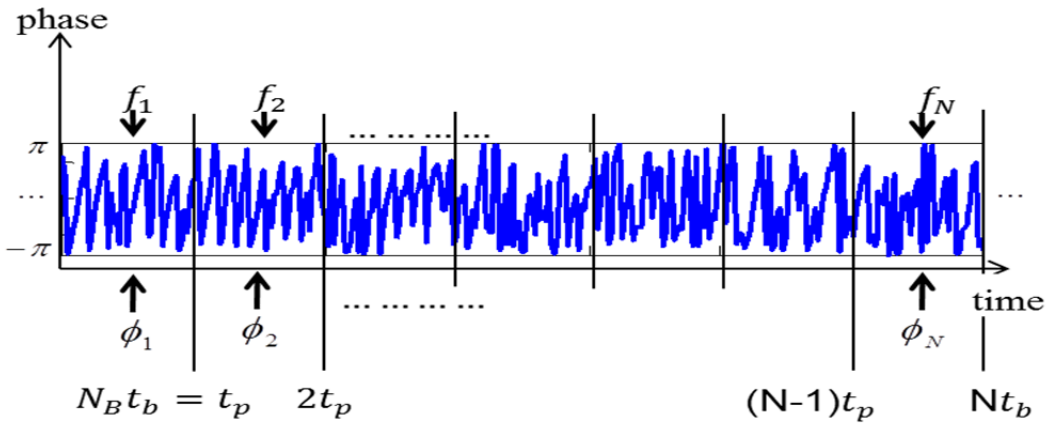

Figure 12. CW waveform using a Frank code with $f_s = 15$ kHz.

Figure 13 shows the power spectrum magnitude of the Costas sequence FSK/PSK after phase modulation that reveals the spread spectrum characteristic of the phase-modulated Costas signal $f = \{3,2,6,4,5,1\}$ kHz. For this signal the sampling

frequency $f_s = 15$ kHz, the subperiod for each frequency is $t_p = 6$ ms (B=167 Hz) and an $N_B = 5$-bit Barker code is used. Figure 14(a,b) shows the ACF and the PACF, respectively, of the FSK/PSK sequence. Note the phase modulation spikes that are present with regular periodicity. Figure 15 shows the PAF and the Doppler side lobes present.

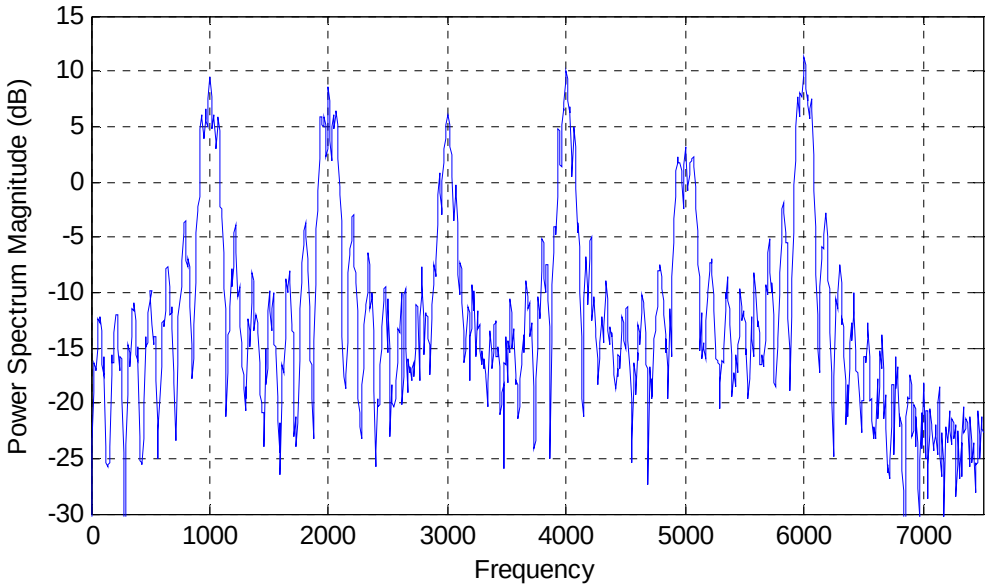

Figure 13. Power spectrum magnitude plot for Costas waveform with 5-bit phase modulation.

It is important to remark that FSK signals provide a higher probability of detection compared to PSK signals but offer many advantages for LPI signaling. Combined with PSK, significant LPI/LPD results can be obtained. The hybrid modulations tend to make the transmitted signal appear as noise-enhancing its LPI nature. These hybrid techniques are a subset of a larger group of radar architectures known as random signal or noise radar, providing a good deal of electronic protection and having a counter-electronic support capability [1].

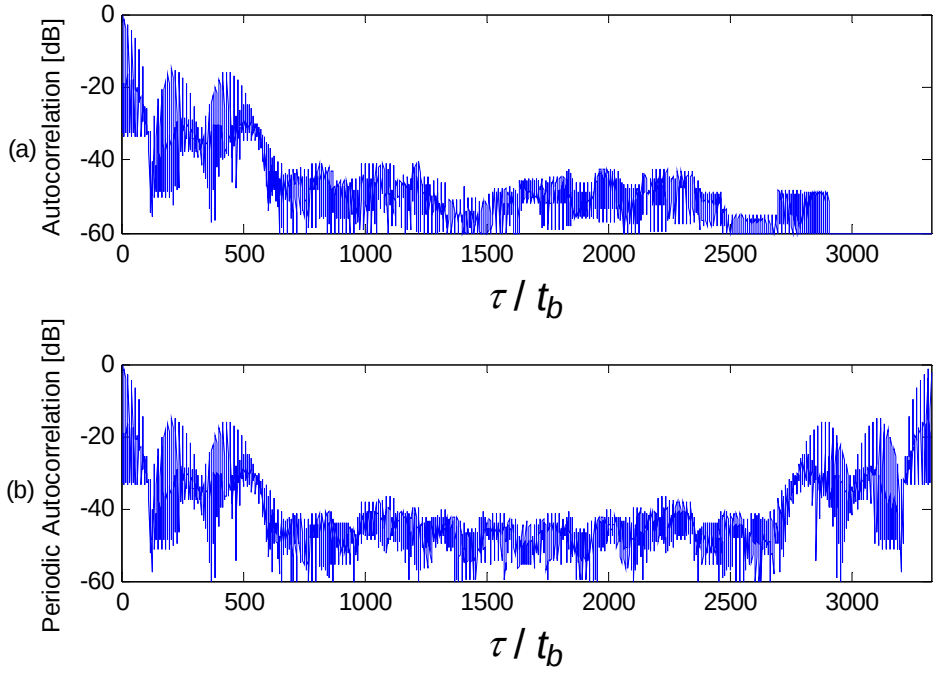

Figure 14. (a) ACF and (b) PACF plot for the Costas sequence with a 5-bit Barker phase modulation.

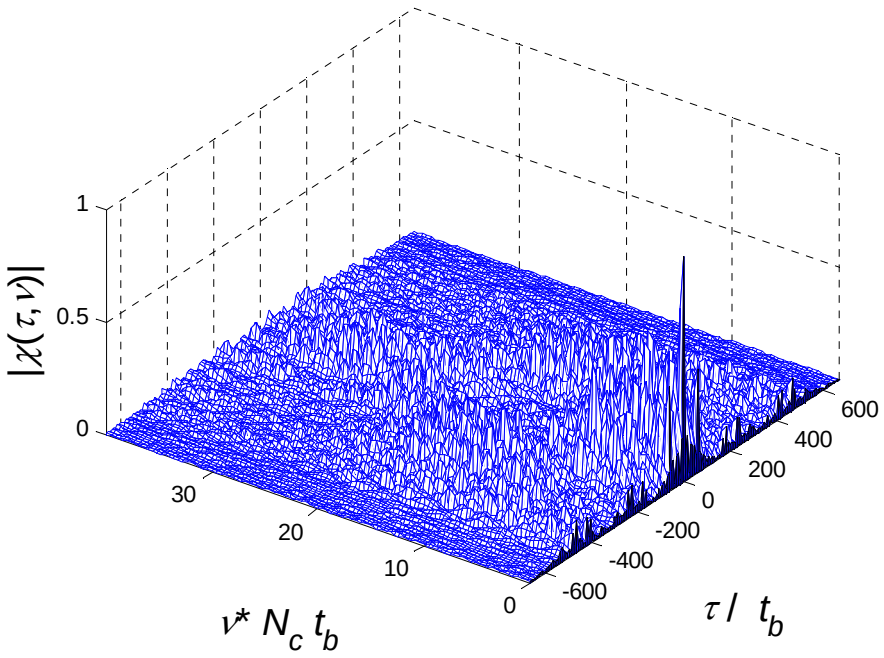

Figure 15. PAF plot for the Costas sequence with a 5-bit Barker phase modulation

THIS PAGE INTENTIONALLY LEFT BLANK

III. GOLAY COMPLEMENTARY SEQUENCES

A. GOLAY DEFINITION

Golay complementary sequences are a pair of finite length of sequences with complementary aperiodic autocorrelation function (AACF) that can be used in radar waveform design. The basic property of Golay complementary sequences is that the sum of the pair of aperiodic autocorrelation functions is zero for all time shifts except at the zero time shift where the sum is twice the length of the code. The property of Golay complementary sequences can be expressed mathematically where a_i and b_i (I = 1,2,…,n) are the pair of binary complementary sequences of code length 2^n. The AACF for the complementary sequences can be express as follows [20]:

$$c_j = \sum_{i=1}^{n-j} a_i a_{i+j} \tag{41}$$

and

$$d_j = \sum_{i=1}^{n-j} b_i b_{i+j} \tag{42}$$

The sum of the pair of AACF can be expressed as

$$c_j + d_j = 0 \rightarrow j \neq 0 \tag{43}$$

and

$$c_0 + d_0 = 2n \tag{44}$$

Golay sequences have been used in, for example, ground penetration radar to improve the range sidelobe levels [21], and netted radar systems [22]. Efficient Golay correlation processors have been reported [23].

Golay gave several recursive and one non-recursive methods for generating complementary sequences. The recursive method used to generate the binary complementary sequences is based on the following algorithm [21]:

$$a_n = \left[a_{n-1}, b_{n-1}\right] \rightarrow b_n = \left[a_{n-1}, -b_{n-1}\right] \tag{45}$$

where the operator [ ] denotes concatenation of sequences, and a_n and b_n represent the complementary binary sequence of length 2^n [7].

B. IMPLEMENTATION

A block diagram of the Golay PSK/FSK radar processor is shown in Figure 16. The first step in generating the transmitted CW waveform is to generate the Costas frequency hopping sequence using, for example, the Welch construction method, described in Chapter II. Next, a sequence of Golay codes a_n is generated (length 2^3) and overlaid on each Costas frequency. Each Golay code takes on one of two values representing a phase change of 0° and 180° of the CW Costas waveform. In the receiver, the AACF is pre-computed for the complementary signal with the Golay sequence b_n. For the receiver waveform (uses a_n), the AACF is computed and the two AACFs are added together. A block diagram of the radar processor is shown in Figure 16.

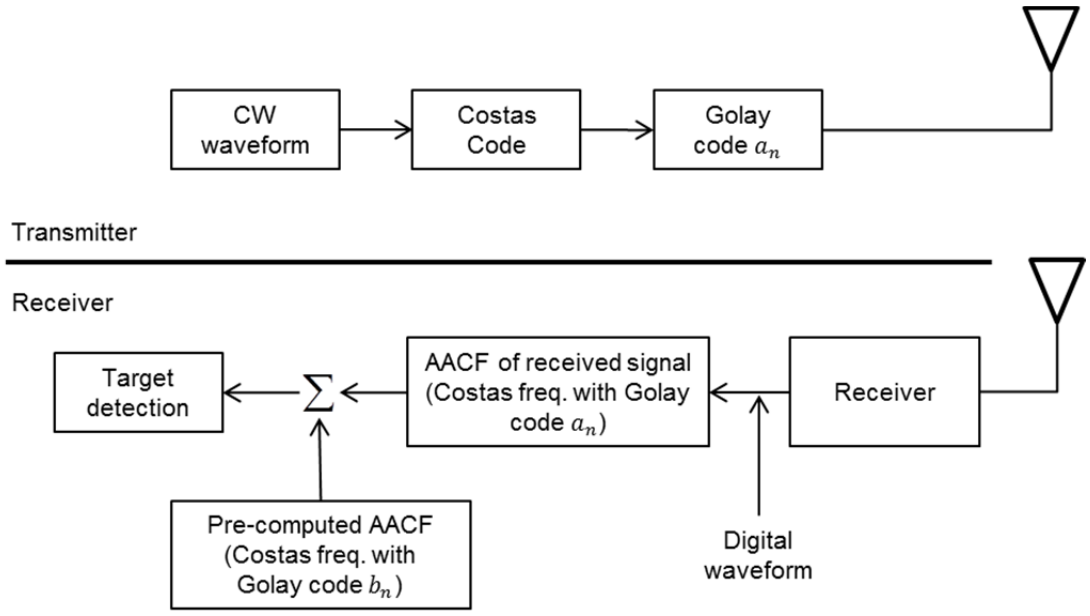

Figure 16. Block diagram of CW emitter using Costas frequency hopping with Golay complementary sequences. From [7].

For this analysis, a CW Costas six-frequency waveform $f_j = [3\ 2\ 6\ 4\ 5\ 1]$ kHz is used for each code period. Each frequency is divided into sub-codes. With the duration of each sub-code $t_p = 7$ ms, the number of cycles within a sub-code for each frequency is $f_c = [21\ 14\ 42\ 28\ 35\ 7]$, respectively. If the receiver samples the return waveform with sampling frequency f_s there are $\lfloor f_s / f_j \rfloor$ samples within each cycle giving a total number of samples within a code period of $N_s = f_c^T \lfloor f_s / f_j \rfloor N_c$ where N_c is the number of sub-codes within a code period [1]. For each waveform five code periods are generated. These parameters were chosen to provide a working example while keeping the computations reasonable.

C. ANALYSIS

Figure 17 shows the AACF and the PACF of the Costas frequency hopping waveform when *n* = 3 ($N_c = 8$) Golay complementary sequence is used $(N_s = 5320)$. The PSL of the waveform is -38 dB, i.e., a 16 dB improvement in PSL is achieved over the Barker $N_c = 13$ waveform. The delay axis is normalized by the sampling period $t_b = 1/f_s = 1/15$ kHz and the AACF and PACF repeat at each code period of N_s samples.

The PSL can be read from Figure 17(a) in where the largest side lobe level is 38 dB down from the peak. Also it can be note from Figure 17(b) that the signal has a PACF = -38 dB (non-zero side lobes), being the ISL= -14 dB.

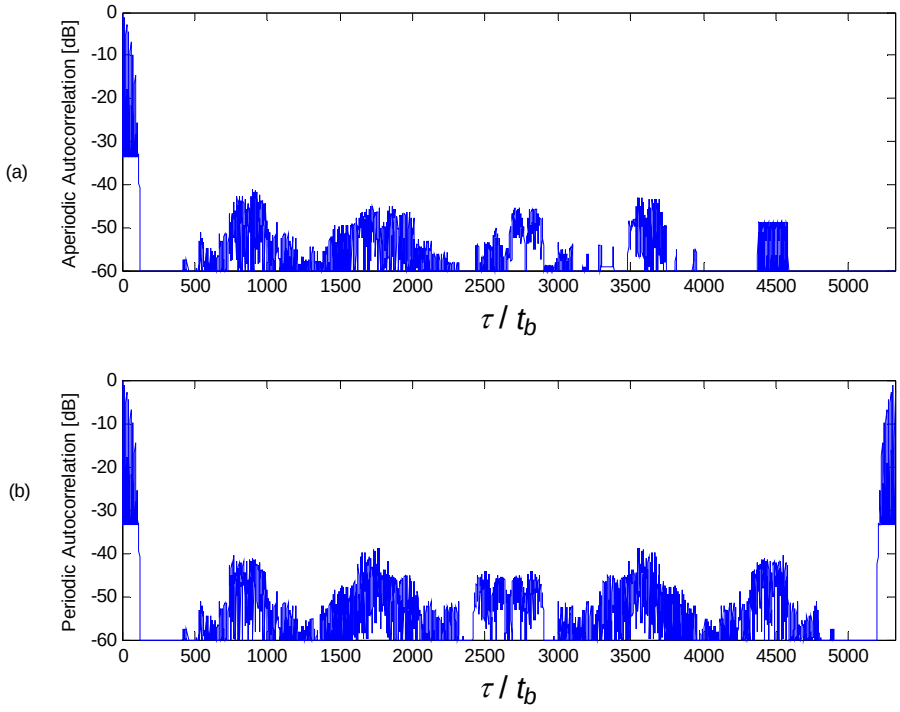

Figure 17. (a) AACF and (b) PACF of Costas FSK waveform using Golay complementary sequence of code length 2^3.

While examining the signal, the axis is normalized by the subcode period t_b and so the PAF from Figure 18, repeats at $N_c b_{sc}$ since the waveform is sampled. That is, dividing this axis by the number of samples per subcode b_{sc} gives the delay axis in terms of the subcode number. Figure 18, as a function of the time delay (τ) and the Doppler frequency shift (ν), is called the ambiguity diagram and by analyzing the delay-Doppler response of the matched filter output, the PDS is approximately equal to -24 dB while the peak time sidelobe is -41 dB.

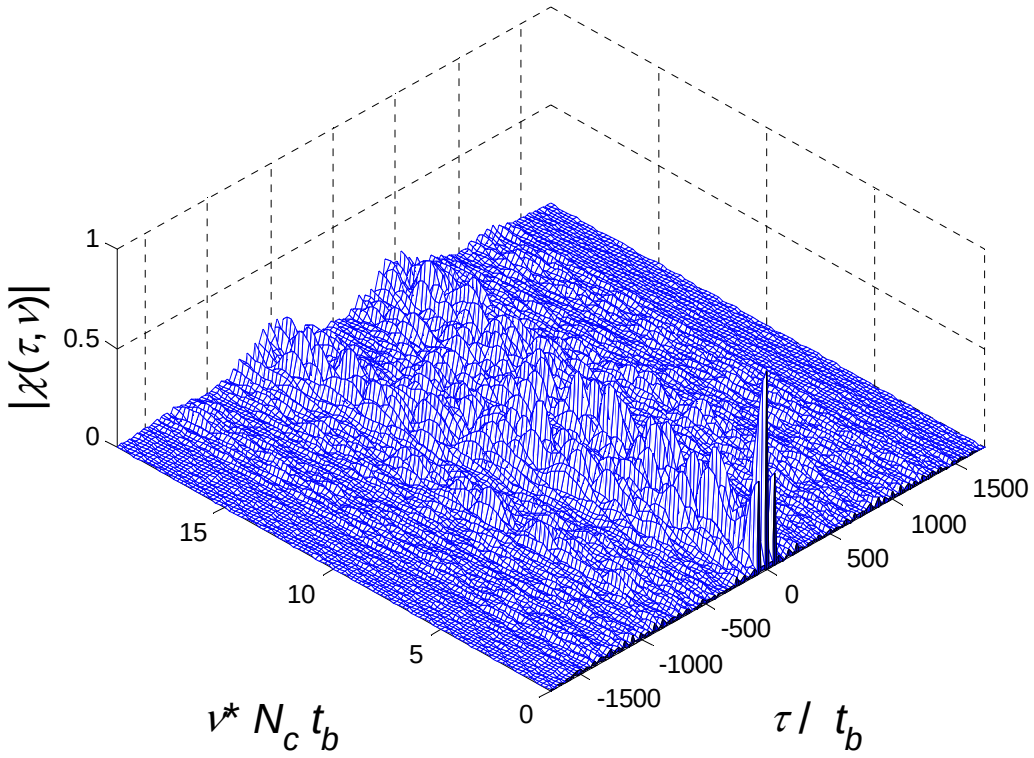

Figure 18. PAF for Costas FSK waveform using Golay complementary sequence of code length 2^3.

In the next chapter, details and implementation of a new Quaternary Periodic Complementary Sequences (QPCS) to encode Costas FSK CW waveforms in order to improve the range (time) sidelobe behavior are presented by applying the techniques described in Chapter II and following the same procedures presented in Chapter III.

THIS PAGE INTENTIONALLY LEFT BLANK

IV. QUATERNARY PERIODIC COMPLEMENTARY SEQUENCE

A. DEFINITION

A new construction method of QPCS was proposed by Ji-Woong Jang et al in [8] using a binary periodic complementary sequence (PCS) set with even period. The proposed method componentwise applies the Grey mapping to a pair of sequences in a binary PCS set, where the only necessary condition is that the employed binary PCS set should have an even period.

For positive integers q and N, let u(t) and v(t) be q-ary sequences over the integer ring $Z_q = \{0,1,...q-1\}$ with period N. Then the PACF of u(t) is defined by

$$R_u(t) = \sum_{t=0}^{N-1} \omega_q^{u(t)-u(t-\tau)} \tag{46}$$

where $0 \le \tau < N$ and ω_q is the complex primitive qth root of unity, e.g., $\omega_4 = \sqrt{-1}$. The periodic cross-correlation function of u(t) and v(t) is defined by

$$R_{uv}(t) = \sum_{t=0}^{N-1} \omega_q^{u(t)-v(t+\tau)} \tag{47}$$

Let $\mathbb{S}$ be a set of M sequences as

$$\mathbb{S} = \left\{ s_i(t) \middle| 0 \le i \le M-1 \right\}. \tag{48}$$

If the sum of all non-trivial periodic autocorrelation functions of $s_i(t) \in \mathbb{S}$ is zero, then $\mathbb{S}$ is called a set of PCS.

$$\sum_{i=0}^{M-1} R_{s_i}(\tau) = \begin{cases} MN, & for\ \tau \equiv \bmod N \\ 0, & for\ \tau \neq \bmod N \end{cases} \tag{49}$$

Let $\phi[r,s]$ be the Gray mapping defined by

$$\phi[r,s] = \begin{cases} 0, & if\ (r,s) = (0,0) \\ 1, & if\ (r,s) = (0,1) \\ 2, & if\ (r,s) = (1,1) \\ 3, & if\ (r,s) = (1,0) \end{cases} \tag{50}$$

Let $r(t)$ and $s(t)$ be binary sequences of period *N*. Then a quaternary sequence *g*(t) is defined by $g(t) = \phi\left[r(t), s(t)\right]$, which can be also expressed as

$$\omega_4^{g(t)} = \frac{1+\omega_4}{2}(-1)^{r(t)} + \frac{1-\omega_4}{2}(-1)^{s(t)}. \tag{51}$$

The cardinality of this complementary sequence set is the same as that of the used binary complementary sequence set. Krone and Sarwate derived the relation between the autocorrelation functions of the binary sequences and the corresponding quaternary sequences in (57) as follows:

Let $r(t)$, $s(t)$, $v(t)$, and $w(t)$ be binary sequences of the same period. Let $g(t)$ and $h(t)$ be quaternary sequences defined by $g(t) = \phi\left[r(t), s(t)\right]$ and $h(t) = \phi\left[v(t), w(t)\right]$, respectively. Then the cross-correlation function (CCF) $R_{gh}(\tau)$ between $g(t)$ and $h(t)$ is given as

$$R_{gh}(\tau) = \frac{1}{2}\left\{R_{rv}(\tau) + R_{sw}(\tau) + \omega_4(R_{rw}(\tau) - R_{sv}(\tau))\right\} \tag{52}$$

For an even integer *N*, let $a(t)$ and $b(t)$ be binary sequences of period *N*. Define a quaternary sequence as

$$q(t) = \phi\left[a(t), b(t + N/2)\right]. \tag{53}$$

Then the PACF of $q(t)$ is calculated as

$$R_q(\tau) = \frac{1}{2}(R_a(\tau) + R_b(\tau)) + \frac{\omega_4}{2}(R_{ab}(\tau + N/2) - R_{ba}(\tau - N/2)). \tag{54}$$

A quaternary sequence set can be constructed from a binary PCS set using the Gray map of a binary sequence and its half-period shift. For an even integer *N*, let B be a binary PCS with *M* sequences of period *N* defined as

$$\mathrm{B} = \left\{b_i(t) \middle| 0 \le i \le M-1\right\} \tag{55}$$

The quaternary sequence set $\mathcal{G}$ is defined as

$$\mathcal{G} = \left\{g_i(t) \middle| 0 \le i \le M-1\right\} \tag{56}$$

where $g_i(t)$ is a quaternary sequence given by

$$g_i(t) = \phi\left[b_i(t), b_i(t + N/2\right]. \tag{57}$$

Then the sequence set $\mathcal{G}$ is a QPCS set.

From the definition of a PCS set, what is important is the sum of all periodic autocorrelation values of all sequences in $\mathcal{G}$ is always zero except for $\tau = 0$.

From (69) and (71) it is obtain

$$\begin{aligned} R_{g_i}(\tau) &= \frac{1}{2}(R_{b_i}(\tau) + R_{b_i}(\tau)) + \frac{\omega_4}{2}(R_{b_i}(\tau + N/2) - R_{b_i}(\tau - N/2)) \\ &= R_{b_i}(\tau) \end{aligned} \tag{58}$$

From Equation (75) it is clear that

$$\sum_{i=0}^{M-1} R_{g_i}(\tau) = \sum_{i=0}^{M-1} R_{b_i}(\tau) = 0 \tag{59}$$

Therefore, $\mathcal{G}$ is a QPCS set [8].

B. IMPLEMENTATION

Following the same steps described in Chapter III implementation section, and considering the example describe in [8], we have:

Let B a binary PCS set of period 16 with 4 sequences defined as

$$\mathrm{B} = \left\{ b_i(t) \middle| 0 \le i \le 3 \right\} \tag{60}$$

where $b_i(t)$ is given as

$$\begin{aligned} b_0(t) &= 0,0,1,0,1,0,0,0,1,0,1,1,0,0,0,1 \\ b_1(t) &= 0,0,0,0,1,0,0,0,0,1,1,0,1,1,1,0 \\ b_2(t) &= 0,0,1,0,1,0,0,0,0,0,1,1,0,1,1,0 \\ b_3(t) &= 0,0,0,0,1,0,0,0,1,1,1,0,1,0,0,1 \end{aligned}$$

Let $\mathcal{G}$ be a set of quaternary sequences according to (72) constructed from B. Then $\mathcal{G}$ is given as

$$\mathcal{G} = \left\{ g_i(t) \middle| 0 \le i \le 3 \right\} \tag{61}$$

where $g_i(t)$ is calculated as

$$g_0(t) = 1,0,2,1,3,0,0,1,3,0,2,3,1,0,0,3$$
$$g_1(t) = 0,1,1,0,2,1,1,0,0,3,3,0,2,3,3,0$$
$$g_2(t) = 0,0,2,1,3,1,1,0,0,0,2,3,1,3,3,0$$
$$g_3(t) = 1,1,1,0,2,0,0,1,3,3,3,0,2,0,0,3$$

And the PACFs of $g_i(t)(0 \le i \le 3)$ are

τ	$R_{g_0}(\tau)$	$R_{g_1}(\tau)$	$R_{g_2}(\tau)$	$R_{g_3}(\tau)$	$\sum R_{g_i}(\tau)$
0	16	16	16	16	64
1	-4	4	0	0	0
2	0	0	0	0	0
3	0	0	0	0	0
4	0	0	0	0	0
5	0	0	-4	4	0
6	0	0	0	0	0
7	4	-4	4	-4	0
8	0	0	0	0	0
9	4	-4	4	-4	0
10	0	0	0	0	0
11	0	0	-4	4	0
12	0	0	0	0	0
13	0	0	0	0	0
14	0	0	0	0	0
15	-4	4	0	0	0

Table 2. PACFs of $g_i(t)$ for B binary PCS set.

C. ANALYSIS

Figure 19 shows the AACF and the PACF of the Costas FH waveform when n = 3 ($N_c = 8$) quaternary complementary sequence is used ($N_s = 5320$). The PSL of the waveform is -39 dB, i.e., a 14 dB and 1 dB improvement in PSL is achieved over the Barker $N_c = 13$ waveform and over the GCS, respectively. The delay axis is also normalized by the sampling period $t_b = 1/f_s = 1/15\,\text{kHz}$ and the AACF and PACF repeat at each code period of N_s samples.

The PSL can be read from Figure 19(a) in where the largest side lobe level is 38 dB down from the peak. This is in agreement with the theoretical result PSL = $20\log_{10}(1/M\pi) = -39$ dB (voltage ratio). Also it can be note from Figure 19(b) that the signal has a PACF = -38 dB (non-zero side lobes), being the ISL= -14 dB.

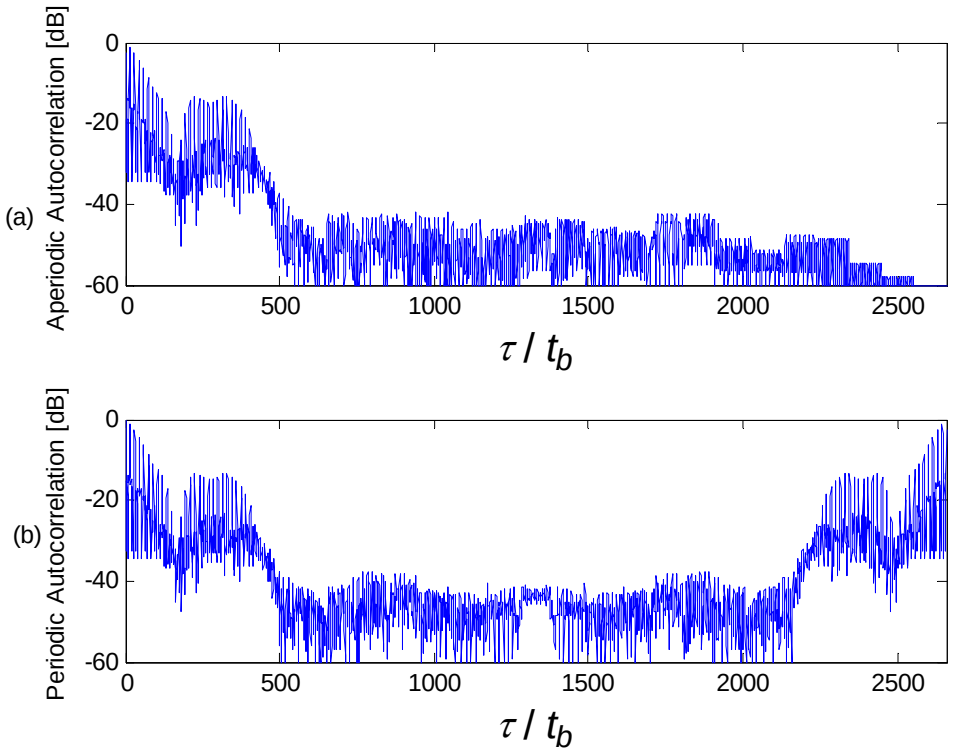

Figure 19. (a) AACF and (b) PACF of Costas FSK waveform using QPCS of code length 2^3.

While examining the signal, the axis is normalized by the subcode period t_b and so the PAF from Figure 20, repeats at $N_c b_{sc}$ since the waveform is sampled. That is, dividing this axis by the number of samples per subcode b_{sc} gives the delay axis in terms of the subcode number. By analyzing the delay-Doppler response of the matched filter output in the ambiguity diagram, the PDS is about -24 dB, being the same results obtained from the GCS analysis.

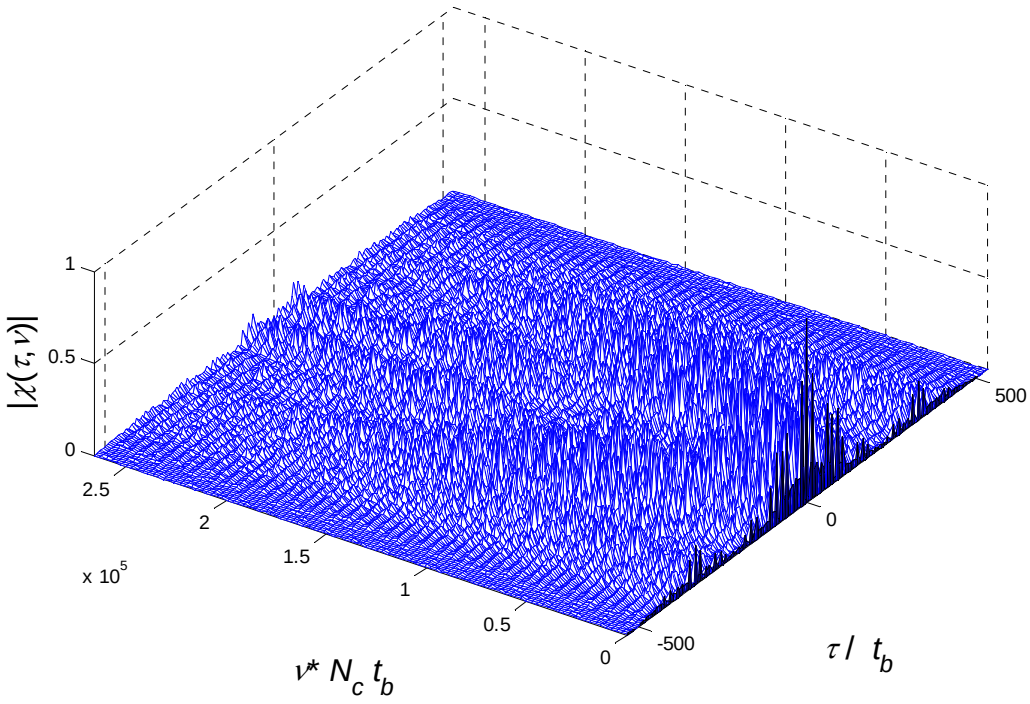

Figure 20. PAF for Costas FSK waveform using QPCS of code length 2^3.

In the next chapter, details and implementation of a new Quaternary Golay Complementary Sequences to encode Costas FSK CW waveforms in order to improve the range (time) sidelobe behavior are presented by applying the techniques described in Chapter II and following the same procedures presented in Chapters III and IV.

V. QUATERNARY GOLAY COMPLEMENTARY SEQUENCES

A. DEFINITION

In their journal paper [9], Zeng et al. gave new constructions methods of the quaternary sequence sets based on the binary sequence sets and Gray mapping. For the aperiodic, periodic, and Z-complementary sequence sets constructed, they considered them as three direct applications of these constructions.

They considered a binary sequence set $U^l = \left(\underline{u}_1^l, \underline{u}_2^l, ..., \underline{u}_M^l\right)$, which consists of M sub-sequences with the same length N. For convenience, for $M = 2M' + 1$ they set

$$x_{s(k-1)+1}^l = \left\{\phi_1(u_{2(k-1)+1}^l(t), u_{2(k-1)+2}^l(t))\right\} \tag{62}$$

and

$$x_{s(k-1)+1}^l = \left\{\phi_2(u_{2(k-1)+1}^l(t), u_{2(k-1)+2}^l(t))\right\} \tag{63}$$

where $1 \le k \le M'$.

Hence, they constructed a quaternary sequence set as follows. For $M = 2M'$, they had

$$\Omega_{11}^l = \left(\underline{x}_1^l, \underline{x}_2^l, \underline{x}_3^l, \underline{x}_4^l, ..., \underline{x}_{2M'-1}^l, \underline{x}_{2M'}^l\right). \tag{64}$$

For $M = 2M' + 1$, they had

$$\Omega_{12}^l = \left(\underline{x}_1^l, \underline{x}_2^l, \underline{x}_3^l, \underline{x}_4^l, ..., \underline{x}_{2M'-1}^l, \underline{x}_{2M'}^l, \underline{x}_M^l\right) \tag{65}$$

where $\underline{x}_M^l = \left\{(-1)^{u_M^l(t)}\right\}$.

The resulting sequence sets have the following properties.

The sum of the ACFs of the quaternary sequence sets in Ω_{11}^l or Ω_{12}^l is

$$\sum_{k=1}^{M} C_{x_k^l, x_k^l}(\tau) = \sum_{k=1}^{M} C_{u_k^l, u_k^l}(\tau) \tag{66}$$

and

$$\sum_{k=1}^{M} R_{x_k^l, x_k^l}(\tau) = \sum_{k=1}^{M} R_{u_k^l, u_k^l}(\tau) \tag{67}$$

Only the aperiodic case and $M = 2M'+1$ are considered due to space limitation and similarity. Was set $r = f = 2(k-1)+1$ and $s = g = 2(k-1)+2$, and $u = v = w = z = u^l$, where $1 \le k \le M'$. Therefore, it is apparent that $C_{x_M^l, x_M^l}(\tau) = C_{u_M^l, u_M^l}(\tau)$. As a consequence

$$\sum_{k=1}^{M} C_{x_k^l, x_k^l}(\tau) = \sum_{k=1}^{M'} \left[C_{x_{2(k-1)+1}^l, x_{2(k-1)+1}^l}(\tau) + C_{x_{2(k-1)+2}^l, x_{2(k-1)+2}^l}(\tau) \right] + C_{x_M^l, x_M^l}(\tau) = \sum_{k=1}^{M} C_{u_k^l, u_k^l}(\tau). \quad (68)$$

The sum if the CCFs between the quaternary sequence sets in Ω_{11}^l and Ω_{11}^h or Ω_{12}^l and Ω_{12}^h has

$$\sum_{k=1}^{M} C_{x_k^l, x_k^h}(\tau) = \sum_{k=1}^{M} C_{u_k^l, u_k^h}(\tau) \quad (69)$$

and

$$\sum_{k=1}^{M} R_{x_k^l, x_k^h}(\tau) = \sum_{k=1}^{M} R_{u_k^l, u_k^h}(\tau) \quad (70)$$

Deriving only the aperiodic case and $M = 2M'$. Let $u = v = u^l$, $w = z = u^h$, $r = f = 2(k-1)+1$, and $s = g = 2(k-1)+2$, where $1 \le k \le M'$, having

$$\sum_{k=1}^{M} C_{x_k^l, x_k^h}(\tau) = \sum_{k=1}^{M'} \left[C_{x_{2(k-1)+1}^l, x_{2(k-1)+1}^h}(\tau) + C_{x_{2(k-1)+2}^l, x_{2(k-1)+2}^h}(\tau) \right] = \sum_{k=1}^{M} C_{u_k^l, u_k^h}(\tau). \quad (71)$$

B. IMPLEMENTATION

Taking from last section the binary sequences U^l and U^h, are now substituted into the GCSS as $GCSS_2(U^l, M, N)$ and $GCSS_2(U^h, M, N)$, respectively. Hence in [9] the authors had the following theorems depending upon *M* being even or odd:

- If $GCSS_2(U^l, M, N)$ is employed, Ω_{11}^l and Ω_{12}^l are $GCSS_4(X^l, M, N)$.
- Let $GCSS_2(U^l, M, N)$ and $GCSS_2(U^h, M, N)$ be the mate to each other. Then so are Ω_{11}^l and Ω_{11}^h or Ω_{12}^l and Ω_{12}^h.
- Let $\left\{ GCSS_2(U^l, M, N) \middle| 1 \le l \le T \right\}$ be the mutually orthogonal (MO) complementary sequence (CS) sets. Then so are:

$$\left\{\Omega_{11}^{l}\,\middle|\,1\le l\le T\right\}=\left\{GCSS_4(X^{l},M,N)\,\middle|\,1\le l\le T\right\}$$
$$\left\{\Omega_{12}^{l}\,\middle|\,1\le l\le T\right\}=\left\{GCSS_4(X^{l},M,N)\,\middle|\,1\le l\le T\right\}.$$

Taking the binary MO CS sets $\left\{GCSS_2(U^{l},4,4)\,\middle|\,1\le l\le 4\right\}$ copied from [24], as follows.

$$\Delta'=\begin{bmatrix}0111 & 1101 & 0111 & 1101\\ 1011 & 1110 & 1011 & 1110\\ 1101 & 0111 & 0010 & 1000\\ 0001 & 1011 & 1110 & 0100\end{bmatrix}$$

where $U^{1}=\left(\underline{u}_1^{1},\underline{u}_2^{1},\underline{u}_3^{1},\underline{u}_4^{1}\right)=(0111,1101,0111,1101)$ and $U^{l}(l=2,3,4)$ are omitted due to similar expressions. Thus they produce the quaternary MO CS sets $\left\{\Omega_{11}^{l}\,\middle|\,1\le l\le 4\right\}=\left\{GCSS_4(X^{l},4,4)\,\middle|\,1\le l\le 4\right\}$ as follows.

$$\Omega'=\begin{bmatrix}1232 & 0323 & 1232 & 0323\\ 3032 & 2123 & 3032 & 2123\\ 3212 & 2303 & 1030 & 0121\\ 1012 & 0103 & 3230 & 2321\end{bmatrix}$$

where $\Omega_{11}^{1}=\left(\underline{x}_1^{1},\underline{x}_2^{1},\underline{x}_3^{1},\underline{x}_4^{1}\right)=(1232,0323,1232,0323)$ and $\Omega_{11}^{l}(l=2,3,4)$ are omitted due to similar expressions.

Taking this implementation into account for this analysis, just U^{1} and U^{2} are being compared as codes, which quaternary MO CS are Ω_{11}^{1} and Ω_{11}^{2}, respectively.

C. ANALYSIS

Figure 21 shows the AACF and the PACF of the Costas frequency hopping waveform when n = 3 ($N_c=8$) quaternary Golay complementary sequence is used ($N_s=5320$). The PSL of the waveform is -41 dB, i.e., a 19 dB and a 2 dB improvement in PSL is achieved over the GCS and the QPCS codes. The delay axis is also normalized by the sampling period $t_b=1/f_s=1/15\,\text{kHz}$ and the AACF and PACF repeat at each code period of N_s samples.

The PSL can be read from Figure 21(a) in where the largest side lobe level is 38 dB down from the peak. This is in agreement with the theoretical result PSL = $20\log_{10}(1/M\pi) = -41\,\text{dB}$ (voltage ratio). Also it can be note from Figure 21(b) that the signal has a PACF = $-41\,\text{dB}$ (non-zero side lobes), being the ISL= $-16\,\text{dB}$.

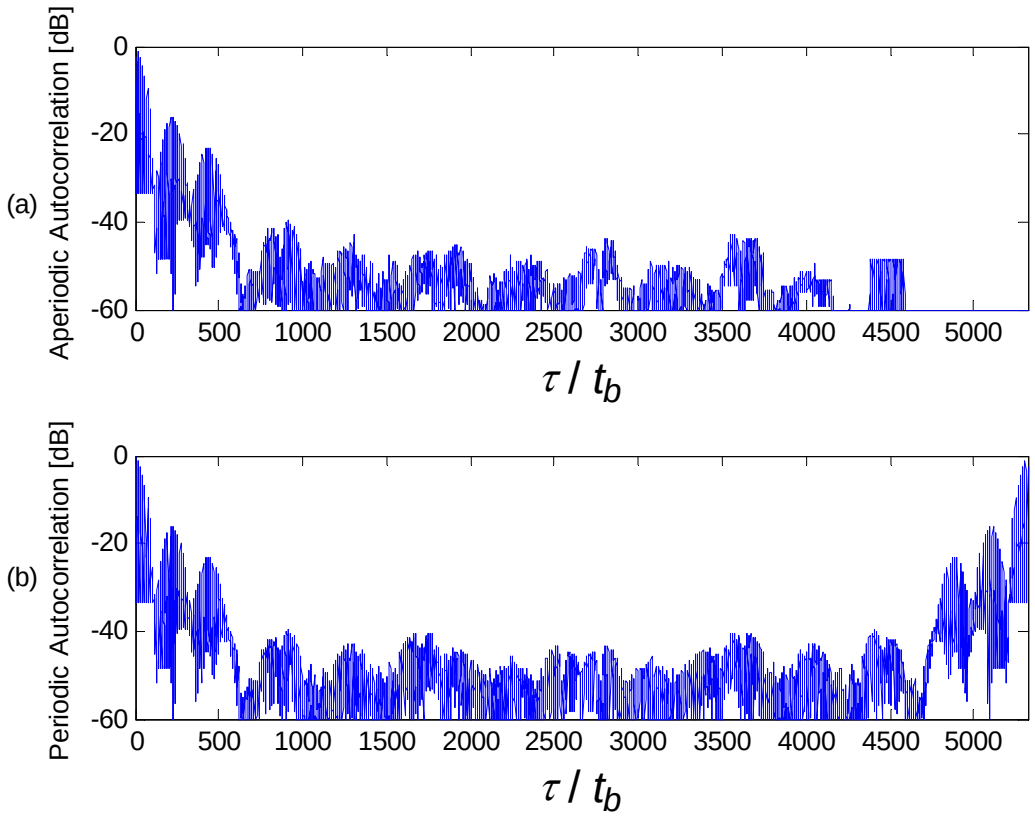

Figure 21. (a) AACF and (b) PACF of Costas FSK waveform using QGCS of code length 2^3.

While examining the signal, the axis is normalized by the subcode period t_b and so the PAF from Figure 22, repeats at $N_c b_{sc}$ since the waveform is sampled. That is, dividing this axis by the number of samples per subcode b_{sc} gives the delay axis in terms of the subcode number. By analyzing the delay-Doppler response of the matched filter output in the ambiguity diagram, the PDS is about $-26\,\text{dB}$, improving in 2 dB the results achieved from the GCS and the GPCS.

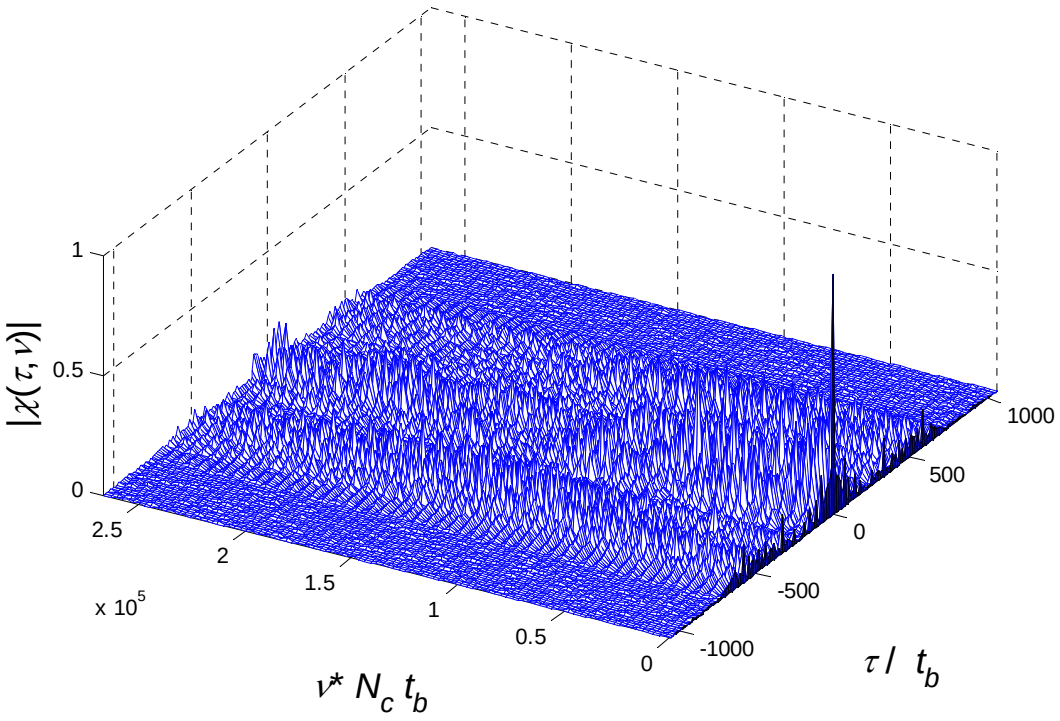

Figure 22. PAF for Costas FSK waveform using QGCS of code length 2^3.

In the next chapter, concluding remarks are examined based on the results obtained. The different performances and particular improvements in the PSL, ISL, and PDS among the implementation of each complementary sequence technique are shown, concluding with future work recommended based on this study.

THIS PAGE INTENTIONALLY LEFT BLANK

VI. CONCLUDING REMARKS

It is relatively easy for an intercept receiver to detect the radiated signals of conventional radars at long ranges. To reduce the radar's detectability to a hostile intercept receiver, its peak power should be made as low as possible. The radiated energy should be spread over a wide angular region over a long time interval, and over a wide frequency band. Digital processing has increased the feasibility and capability of the ubiquitous radar [12].

The LPI systems' rapid development is in response of the rapid change in the signal environment and the increase in capabilities of modern intercept receivers with one goal in common, detect and locate a radar emitter without being jammed. Every day these radars exhibit improvements in both power usage and duty cycles, which is why for every improvement in LPI radar, improvements in intercept receiver design can be expected [1].

Hybrid modulations presented in this study tend to make the transmitted CW waveform appear as noise-enhancing its LPI nature. These hybrid techniques are a subset of a larger group of radar architectures know as random signal or noise radar. Random signal radar techniques can derive target detections using correlation, spectrum analysis, or anticorrelation. Because of the random nature of the transmitted waveform, random signal radar also provides a good deal of electronic protection and has a counter-electronic support capability [1].

The improvement of the range (time) sidelobe behavior based on the three new classes of PSK/FSK CW signals for LPI radar applications are summarized in Table 3 and are compared to the P4 polyphase code, where the AACF and PACF are shown in Figure 23(a) and 23(b), respectively and the PAF in Figure 24. The use of these complementary sequences to phase modulated a Costas FSK waveform and to evaluate the periodic ambiguity properties, allows the comparison of the range (time) offset and Doppler offset sidelobe performance by confronting the values of the PSL, ISL, and PDS in dB.

SEQUENCE	PSL	ISL	PDS
GCS	-38 dB	-14 dB	-24 dB
QPCS	-39 dB	-14 dB	-24 dB
QGCS	-41 dB	-16 dB	-26 dB
P4 code	-23 dB	-10 dB	-18 dB

Table 3. Results of PSL, ISL, and PDS from the complementary sequences and comparison with the P4 polyphase modulated code.

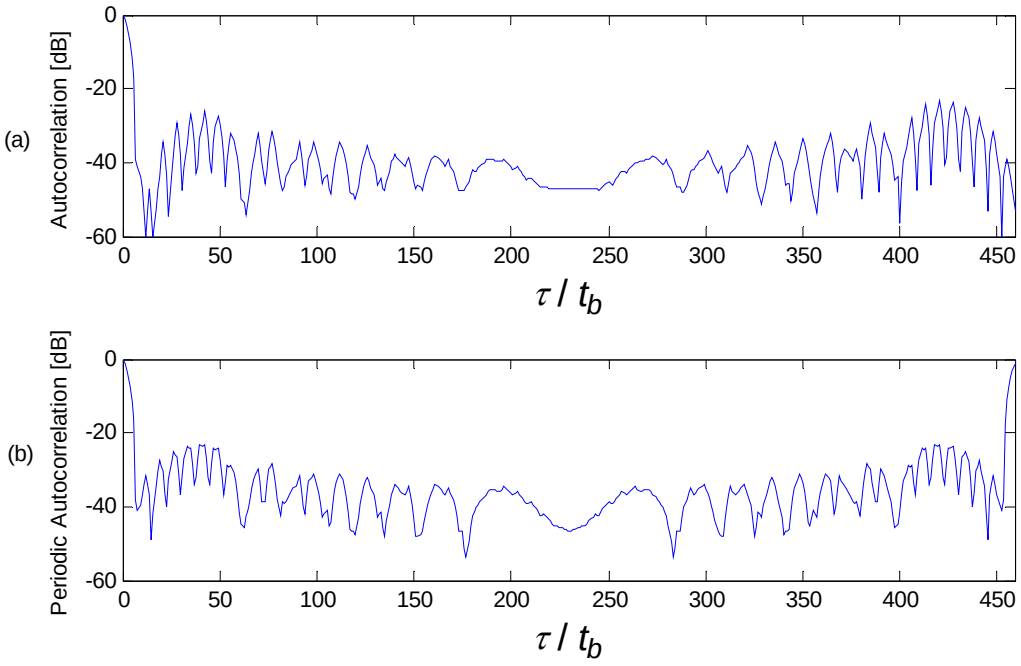

Figure 23. (a) AACF and (b) PACF of P4 code of length 2^3.

Increasing the number of code periods *N* used in the receiver can help to decrease the Doppler side lobes as well as the time side lobes in the ACF. By using more copies of

the reference signal within the correlation receiver, the delay-Doppler sidelobe performance improves, but comes at the expense of a more complex receiver and correlation processor.

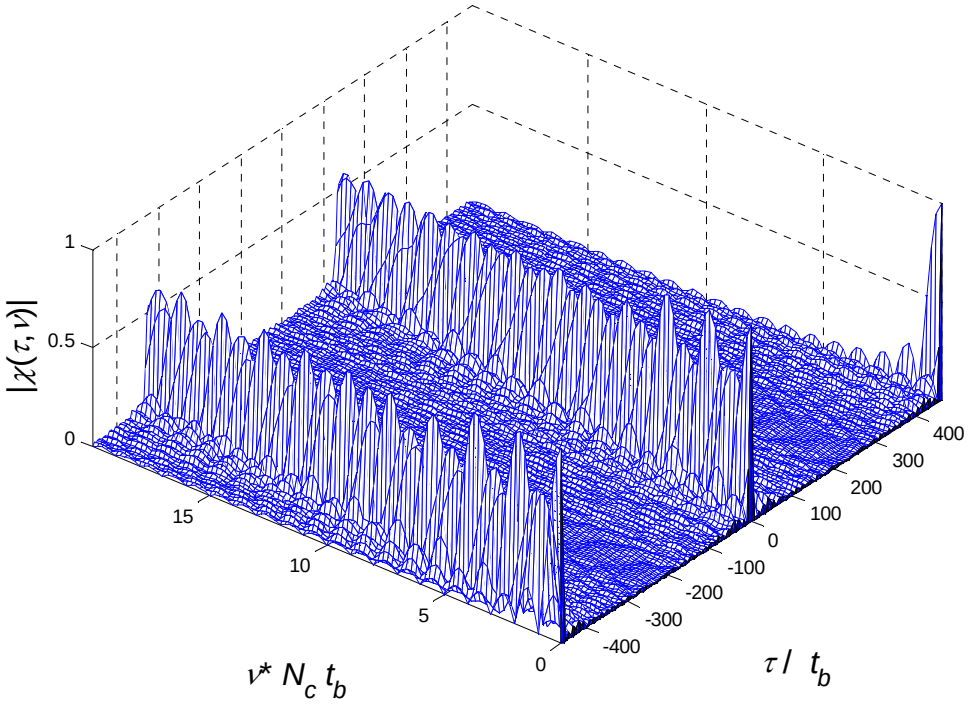

Figure 24. PAF P4 code of length 2^3.

By implementing different complementary sequence sets, improvements in sidelobe performance are also achieved while keeping the same number of code periods avoiding the expense mentioned above. These techniques can be implemented in LPI radar technology to achieve its LPI goals.

The simulations to achieve the data were performed with MATLAB-based software, using a graphic user interface written by Mozeson E. and Levanon N. of the Department of Electronic Engineering – Systems from Tel Aviv University, developing new algorithms by applying recursive methods to generated the different complementary sequences, following the same procedure establish by Pace P. E. and Ng C. Y. in [7] .

Future investigations with different complementary sequence techniques could be considered, such as quaternary Z-complementary sequences, different mutually orthogonal complementary sets of sequences, among others, in order to establish a more robust comparable matrix and to overcome both the mathematical and simulation challenges they present.

VII. LIST OF REFERENCES

[1] P. E. Pace, *Detecting and Clasifying Low Probability of Intercept Radar*, 2nd ed., Norwood, MA: Artech House, 2009.

[2] L. I. Ruffe and G. F. Stott, "LPI considerations for surveillance signals," in *Proc. of the Internation Conference on Radar*, Bringhton, U.K,, 1992.

[3] J. P. Lee, "Intercept of LPI radar signals," Defense Research Establishment, Ottawa, 1991.

[4] J. P. Costas, "A study of a class of detection waveforms having nearly ideal range-Doppler ambiguity properties," *Proc. of th IEEE*, vol. 72, no. 8, pp. 996–1009, August 1984.

[5] J. P. Donohoe and F. M. Ingels, "The ambiguity properties of FSK/PSK signals," *Record of the IEEE 1990 International Radar Conference*, pp. 268–273, 7–10 May 1990.

[6] B. J. Skinner, J. P. Donohoe and F. M. Ingels, "Simplified performance estimation of FSK/PSK hybrid signaling radar systems," *Proc. of the IEEE 1993 National Aerospace and Electronics Conference*, vol. 1, pp. 255–261, 24–28 May 1993.

[7] P. E. Pace and C. Y. Ng, "Costas CW frequency hopping radar waveform: peak sidelobe improvement using Golay complementary sequences," *Electron. Lett.*, vol. 46, no. 2, pp. 1–2, 21st January 2010.

[8] J. W. Jang, Y. S. Kim , S. H. Kim, D. W. Lim and D. W. Lim, "New construction methods of quaternary periodic complementary sequence sets," *Advances in Mathematics of Communications*, vol. 4, no. 1, pp. 61–68, 2010.

[9] F. Zeng, X. Zeng, Z. Zhang, X. Zeng, G. Zuan and L. Xiao, "New construction method for Quaternary Aperiodic, Periodic, and Z-Complementary Sequence Sets," *Journal of Communications and Networks*, vol. 14, no. 3, pp. 232–234, June 2012.

[10] C. A. Balanis, *Antenna Theory Analysis and Design*, New York: Harper and Row, Publishers, 1982.

[11] N. Levanon, *Radar Principles*, New York: John Wiley & Sons, 1988.

[12] M. I. Skolnik, *Introduction to Radar Systems*, 3rd ed., Boston: McGraw Hill, 2001, p. 331.

[13] N. Levanon, "CW alternatives to the coherent pulse train," *IEEE Trans. on Aerospace and Electronic Systems*, vol. 29, no. 1, pp. 250–254, Jan. 1993.

[14] N. Levanon and A. Freedman, "Periodic ambiguity function of CW signals with perfect periodic autocorrelation," *IEEE Trans. on Aerospace and Electronic Systems*, vol. 28, no. 2, pp. 387–395, April 1992.

[15] B. Getz and N. Levanon, "Weight effects on the periodic ambiguity function," *IEEE Trans. on Aerospace and Electronic Systems*, vol. 31, no. 1, pp. 182–193, Jan. 1995.

[16] W.-K. Lee and H. D. Griffiths, "A new pulse compression technique generating optimal uniform range sidelobe and reducing integrated sidelobe level," *Record of the IEEE International Radar Conference*, pp. 441–446, 2000.

[17] S. W. Golomb and R. A. Scholtz, "Generalized Barker Sequences," *IEEE Trans. on Information Theory*, Vols. IT-11, no. 4, pp. 533–537, Oct. 1965.

[18] R. L. Frank, "Polyphase codes with good nonperiodic correlations properties," *IEEE Trans.*, no. IT-9, pp. 43–45, 1963.

[19] B. L. Lewis, F. F. Kretshmer and W. W. Shelton, *Aspects of Radar Signal Processing*, Norwood, MA: Artech House, 1986.

[20] M. Golay, "Complementary series," *IRE Trans., IT-7*, pp. 82–87, 1961.

[21] A. V. Alejos, M. Dawood, H. U. Mohammed, M. G. Sanchez, R. P. Jedlicka and I. Cuinas, "Low sidelobe level radar techniques using Golay based coded sequences," in *IEEE Int. Symp. on Antennas and Propagation*, San Diego, CA, USA, July 2008.

[22] Y. Paichard, "Orthogonal multicarrier phase coded signal for netted radar systems," in *IEEE Int. Waveforms Diversity and Design Conference*, Kissimmee, FL, USA, February 2009.

[23] S. Z. Budisin, "Efficient pulse compressor for Golay complementary sequences," *Electron. Lett.*, vol. 27, no. (3), pp. 219–220, 1991.

[24] C. C. Tseng and C. L. Liu, "Complementary sets of sequences," *IEEE Trans. Inf. Theory*, Vols. IT-18, no. 5, pp. 644–652, Sept. 1972.

INITIAL DISTRIBUTION LIST

1. Defense Technical Information Center
   Ft. Belvoir, Virginia

2. Dudley Knox Library
   Naval Postgraduate School
   Monterey, California

3. Dr. Andres Larraza
   Department of Physics
   Naval Postgraduate School
   Monterey, California

4. Prof. Pace E. Phillip
   Department of Electrical and Computer Engineering
   Naval Postgraduate School
   Monterey, California

5. Prof. Richard Harkins
   Department of Physics
   Naval Postgraduate School
   Monterey, California

6. Prof. Nadav Levanon
   Department of Electrical Engineering – Systems
   Tel Aviv University
   Tel Aviv, Israel

7. Commander Oscar D. Tascon
   COTECMAR
   Cartagena, Colombia